THE EFFICIENCY OF A VISCOUS FLOW COMPRESSOR

A THESIS

Presented to

The Faculty of the Division of Graduate

Studies and Research

By

John Spencer Caldwell, Jr.

In Partial Fulfillment

of the Requirements for the Degree

Master of Science in Mechanical Engineering

Georgia Institute of Technology

June, 1973

THE EFFICIENCY OF A VISCOUS FLOW COMPRESSOR

Approved:

Gene T. Colwell, Chairman

Samuel V. Shelton

M. R. Carstens

Date Approved by Chairman: May 29, 1973

ACKNOWLEDGMENTS

My sincere appreciation is extended to Dr. Gene T. Colwell, my advisor, for his valuable assistance during the preparation of this thesis. I would also like to thank the other members of my committee, Dr. Sam V. Shelton and Dr. M. R. Carstens, for their time and assistance.

Special gratitude is due to my wife, Judy, for her patience during these two years of graduate study.

Finally, I would like to thank the United States Army and those who support it for giving me the opportunity to pursue a graduate education.

TABLE OF CONTENTS

Table of Contents Continued

LIST OF TABLES

LIST OF ILLUSTRATIONS

SUMMARY

The instrumentation, seal design, and wheel disc profile of a previously investigated viscous flow compressor were modified, and the characteristics of the compressor were experimentally determined. Instrumentation modifications enabled the power input to the drive turbine to be determined; therefore mechanical power losses in the experimental apparatus were evaluated. The new seal design featured aluminum seal blocks with detachable sets of seal teeth with significantly reduced (compared to previous designs) surface area vis-a-vis the wheel discs. Two seal teeth materials, teflon and inconel X-750, were tested at compressor rotational speeds up to 35,000 rpm and 42,000 rpm, respectively. The disc edges were tapered to reduce flow losses and therefore increase the efficiency.

Pressure rise versus flow rate, adiabatic compression efficiency, mechanical power losses, and internal efficiency were determined for the compressor incorporating the new seal design and tapered-edge wheel discs. These results were compared to the theoretical and experimental results obtained in a previous investigation of the compressor conducted prior to the above modifications. This comparison indicated poorer compressor performance with both types of seal teeth, due to the ineffective sealing capability and lack of durability of the seal design.

No evaluation of the effects of the tapered wheel discs could be made based on the results of this investigation due to poor seal performance.

Valuable information, previously unrecorded, was obtained which can be applied to future viscous flow compressor design. Inconel was found to have potential as a seal material, whereas teflon was shown to be unsuitable. The efficiency of this compressor was found to be greatly reduced by detrimental heat transfer effects from the shaft bearing and by excessively high seal drag and disc friction mechanical power losses in the compressor. As a result of these discoveries, the design of a relatively efficient viscous flow compressor is closer to reality.

GLOSSARY OF ABBREVIATIONS*

C_p = specific heat at constant pressure (BTU/lbm ^{o}R)

f = friction factor for laminar or turbulent flow

g_c = gravitational constant (32.174 ft/lbm/lbf - sec^2)

H = height of the rotor slots

h_{lfe} = differential pressure drop across the laminar flow element (in. of H_2O)

h_{line} = differential pressure drop across the orifice plate in the compressed air feed line (in. of H_2O)

J = heat equivalent of work (778 ft-lbf/BTU)

N = compressor rotational speed (revolutions per minute)

P_a = compressor interior pressure (lbf/in^2)

P_b = compressor interior pressure (lbf/in^2)

P_e = drive turbine exit pressure (lbf/in^2)

P_i = drive turbine inlet pressure (lbf/in^2)

P_1 = ambient pressure (inches of mercury)

P_3 = diffuser exit pressure (inches of mercury)

Q_{lfe} = volume flow rate through the laminar flow element (ft^3/min)

Q_{line} = volume flow rate in the compressed air feed line (ft^3/hr)

---

*Abbreviations not listed here are defined in the text and in the sample calculations.

Glossary of Abbreviations Continued

Re	=	Reynolds number
T_a	=	compressor interior temperature (^{o}F)
T_b	=	compressor interior temperature (^{o}F)
T_e	=	drive turbine exit temperature (^{o}F)
T_i	=	drive turbine inlet temperature (^{o}F)
T_{lfe}	=	temperature of the fluid entering the laminar flow element (^{o}F)
T_1	=	ambient temperature (^{o}F)
T_2	=	diffuser inlet temperature (^{o}F)
T_3	=	diffuser exit temperature (^{o}F)
V	=	absolute velocity, designated at various points in the flow by subscripts (ft/sec)
W	=	width of the grooves in the wheel (inches)

CHAPTER I

INTRODUCTION

1-1. The Viscous Flow Compressor

The viscous flow compressor is a type of turbomachine which increases the pressure of the flowing fluid by means of the viscous drag forces acting between the multiple-disc wheel and the fluid. In conventional compressors the pressure rise is accomplished by a change in the fluid momentum caused by flow through a system of blades and vanes.

Also in conventional compressors, the flow of the fluid is either axial, radial, or in some cases a mixture of the two. The flow path in the compressor in this study was entirely circumferential. The fluid was guided into the grooves on the periphery of the wheel by means of seal "teeth" which extended into the grooves. The fluid was then dragged around a portion of the periphery of the wheel and extracted from the grooves by another set of seal teeth. See Figure 1.

1-2. Statement of the Problem

The purpose of this investigation was to modify the instrumentation, wheel disc profile, and seal design of the viscous flow compressor previously studied in the School of Mechanical Engineering at the Georgia Institute of Technology, and to determine the performance characteristics of the compressor incorporating these modifications. Particular attention was given to the determination of the efficiency

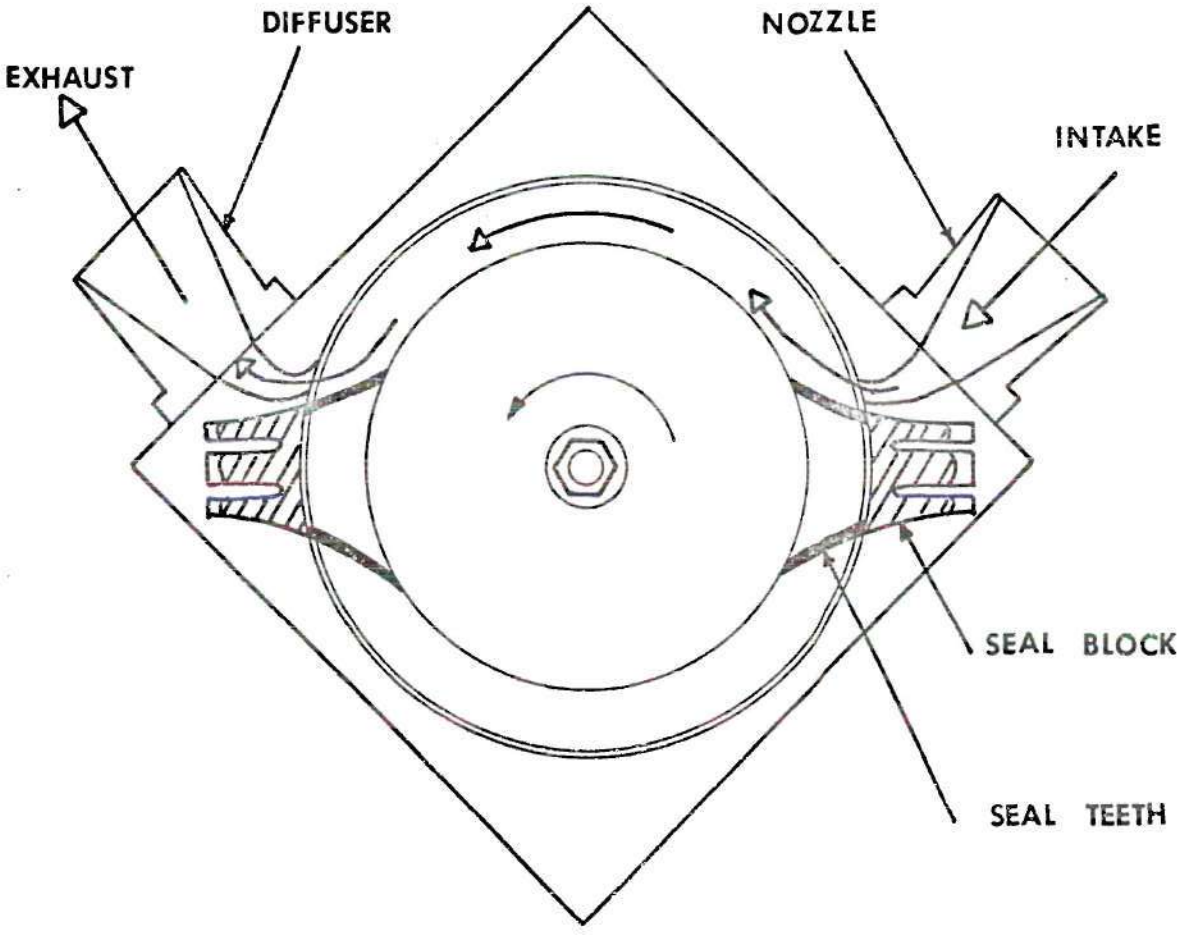

Figure 1. Compressor Flow Path.

of the compression process.

The performance characteristics of this compressor depend primarily on the effectiveness of the seals. If the seals allow excessive leakage, the pressure rise, volume flow rate, and compression efficiency will be severely reduced. In order to function effectively, the seals must be manufactured to close tolerances, yet must not cause significant frictional drag on the compressor wheel. The seal material must possess high strength and be resistant to frictional wear and high temperature damage.

1-3. Literature Survey

Investigations of turbomachinery with multiple disc rotors date back to the early twentieth century. The first United States patents on this type of rotor were issued to N. Tesla in 1913 (1).[1] For this reason the blading is often referred to as Tesla blading. Tesla's experimental turbines did not utilize an entirely circumferential flow path as did the compressor in this investigation. The fluid (air or steam) entered on the wheel periphery and followed an inward spiral path to exit at exhaust holes near the center of the wheel discs. In addition, his turbines operated at speeds up to 20,000 rpm (525 feet per second tip speed) (2), versus a speed of 42,000 rpm (1280 feet per second tip speed) attained by the compressor in this study.

The first experimental work on this type of turbomachinery at the Georgia Institute of Technology was completed in 1952, by J. Armstrong (2). He studied the characteristics of a turbine utilizing a seven

---

[1] Numbers in parenthesis designate references at the end of the study.

inch diameter rotor with ten tapered edged discs, and utilizing the same flow path as described above. This experimental turbine developed a maximum output of 1.11 horsepower at 8300 rpm and 118 psig inlet pressure.

A series of analytical and experimental investigations on multiple-disc rotor turbomachinery was initiated at Arizona State University in 1958, under the direction of Dr. Warren Rice. These studies were undertaken to determine the feasibility of using pumps, compressors, and turbines incorporating this type of rotor and flow path for practical engineering applications. The first results of these studies were published in 1963 (3), and Dr. Rice concluded that rotors of this type did have potential for practical applications even though they might not be as efficient as conventional rotors. Further results of the work by Dr. Rice were published in 1965 (4).

W. Gordon, a student of Dr. Rice's, published a thesis (5) on the performance of a disc-type air compressor in 1965. He used a rotor six inches in diameter composed of 77 smooth, flat edged, stainless steel discs. The interior discs were 0.020 inches thick and were separated by spacers which were 0.020 inches thick. The exterior discs were 0.250 inches thick. Eight air inlet slots were provided in the rotor hub near the shaft. Gordon experimentally determined power, pressure rise, and hydraulic efficiency as functions of volume flow rate for constant speed. His range of operation was from 5,000 rpm to 18,000 rpm (131 to 472 feet per second tip speed). The maximum pressure rise that he attained was 36 inches--H_2O (2.57 in.-H_g) at zero flow rate, 18,000 rpm. He defined hydraulic efficiency

as the ratio of the net energy added to the fluid (flange to flange) to the energy supplied to the rotor. He achieved a maximum hydraulic efficiency of 28 per cent at a flow rate of 188 cfm and a speed of 14,000 rpm.

The rotors used in all of the investigations at Arizona State University consisted of various numbers of discs fastened together with spacers between them. The flowing medium entered the apparatus through holes near the center of the rotor and followed an outward spiral path between the discs. The exhaust was at the periphery of the rotor. This path was reversed in the case of the inward flow turbine in reference four. No attempt was made to extract the fluid from the rotor by means of a seal. The principle disadvantage of the above rotor and characteristic flow path was the high flow loss incurred as the fluid made a 90 degree turn at the intake holes. These losses increased significantly as the rotational speed was increased.

In an effort to improve the performance of turbomachinery utilizing Tesla blading and to develop a single wheel gas turbine, several analytical and experimental investigations have been conducted at Georgia Tech under the supervision of Dr. Gene T. Colwell. In these studies, the flow path described in the preceeding paragraph was modified to become an entirely circumferential path. Intake and exhaust seals were added to guide the fluid. These modifications eliminated the 90 degree turn in the flow path of previous studies. A schematic diagram of the new flow path was shown in Figure 1.

Traviss (6) developed the theoretical analysis for this new flow path. In his development, he assumed the flow to be one-

dimensional, compressible, and adiabatic. He considered the laminar and turbulent flow regimes. He also wrote a computer program to predict the theoretical performance of a viscous flow compressor. At a rotational speed of 42,000 rpm, he predicted a maximum pressure rise of approximately 21 inches of mercury.

Dusadeenoad (7) published the first results of experimental work on a viscous compressor utilizing totally circumferential flow with seals which guided the air into the grooves and scavenged it out after it was compressed. The seven inch diameter wheel was made of titanium and the grooves were machined into the periphery of the wheel. The edges of the discs were flat. The seals were constructed of solid blocks of graphite which were worn-in by the wheel itself. Pressure rise, temperature change, and adiabatic compression efficiency versus flow rates were theoretically and experimentally determined. Geometry effects were also studied theoretically. The compressor was operated at speeds up to 42,000 rpm. The maximum pressure rise attained was 15.5 inches of mercury at 42,000 rpm and zero flow rate. The maximum adiabatic efficiency attained was about 27 per cent at 24,000 rpm and a flow rate of 10 standard cubic feet per minute (scfm).

W. Clarke (8) did further experimental work with the same wheel and basic equipment as Dusadeenoad. He used seals constructed in sandwich fashion with alternating sheets of Brunswick DH-242* stainless steel metal fiber acting as the teeth and spacers made of 3003-H14 aluminum. The compressor was operated at speeds up to 45,000 rpm. A

---

*Trademark of the Brunswick Corporation, Technical Products Division, 69 West Washington Street, Chicago, Illinois 60602.

maximum pressure rise of 10 inches of mercury was attained at 45,000 rpm and zero flow rate. The seals were almost completely destroyed after nine hours of operation.

CHAPTER II

INSTRUMENTATION AND EQUIPMENT

2-1. Experimental Apparatus

The experimental apparatus used in this investigation was essentially the same as that used in the work by Dusadeenoad (7), with the exception of the following modifications:

1. The periphery of each of the discs on the titanium wheel was ground to a tapered profile as shown in Figure 2.

2. The basic seal design was changed from a solid graphite construction to a two piece configuration. The new seal design featured aluminum seal blocks with detachable seal teeth. For the purpose of this study, one set of seal teeth was made of teflon and another set was made of inconel X-750. The wearing surface of the seal teeth vis-a-vis the wheel discs was drastically reduced by this design. The basic features of this seal design is shown in Figure 3.

3. The exit diffuser was replaced by another diffuser which had a throat area that matched the exhaust hole in the compressor casing. In addition, the flow passages in the intake nozzle and exhaust diffuser were filed to allow a smoother transition from a circular cross-sectional area to a rectangular one.

4. Instrumentation was added to enable the investigator to determine the power input to the drive turbine.

A schematic diagram of the experimental apparatus for this study is shown in Figure 4.

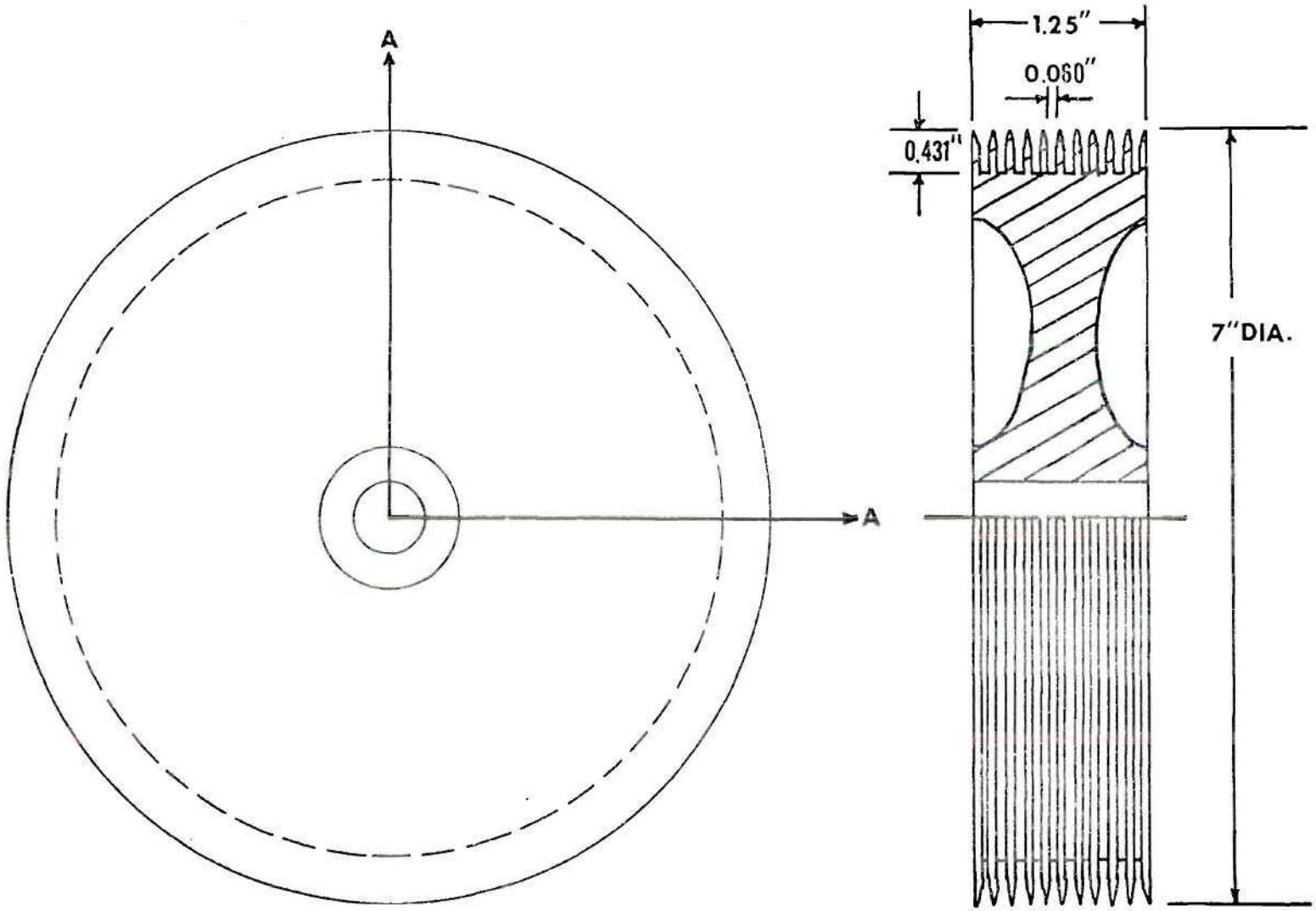

Figure 2. Wheel Profile.

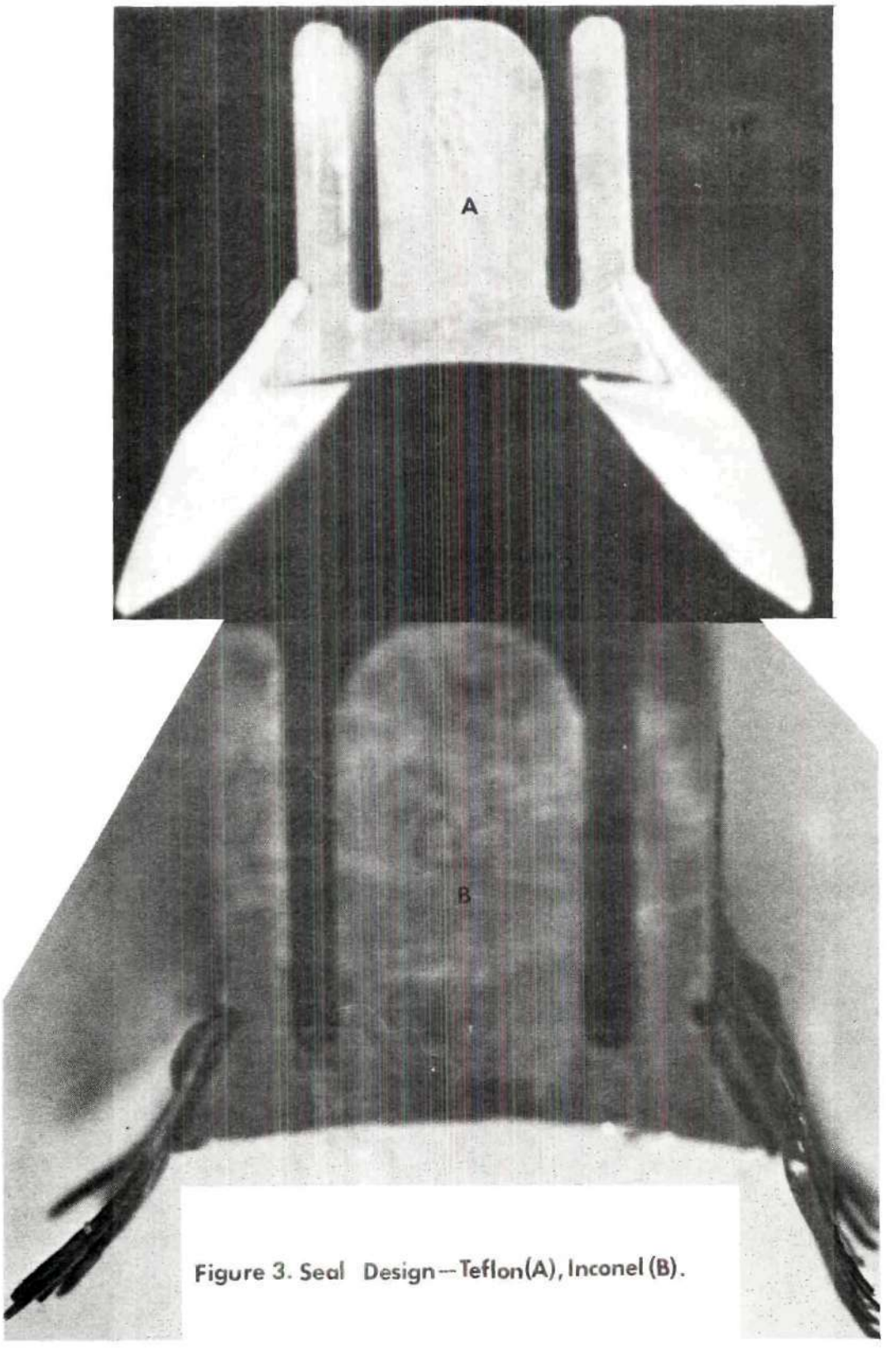

Figure 3. Seal Design—Teflon(A), Inconel (B).

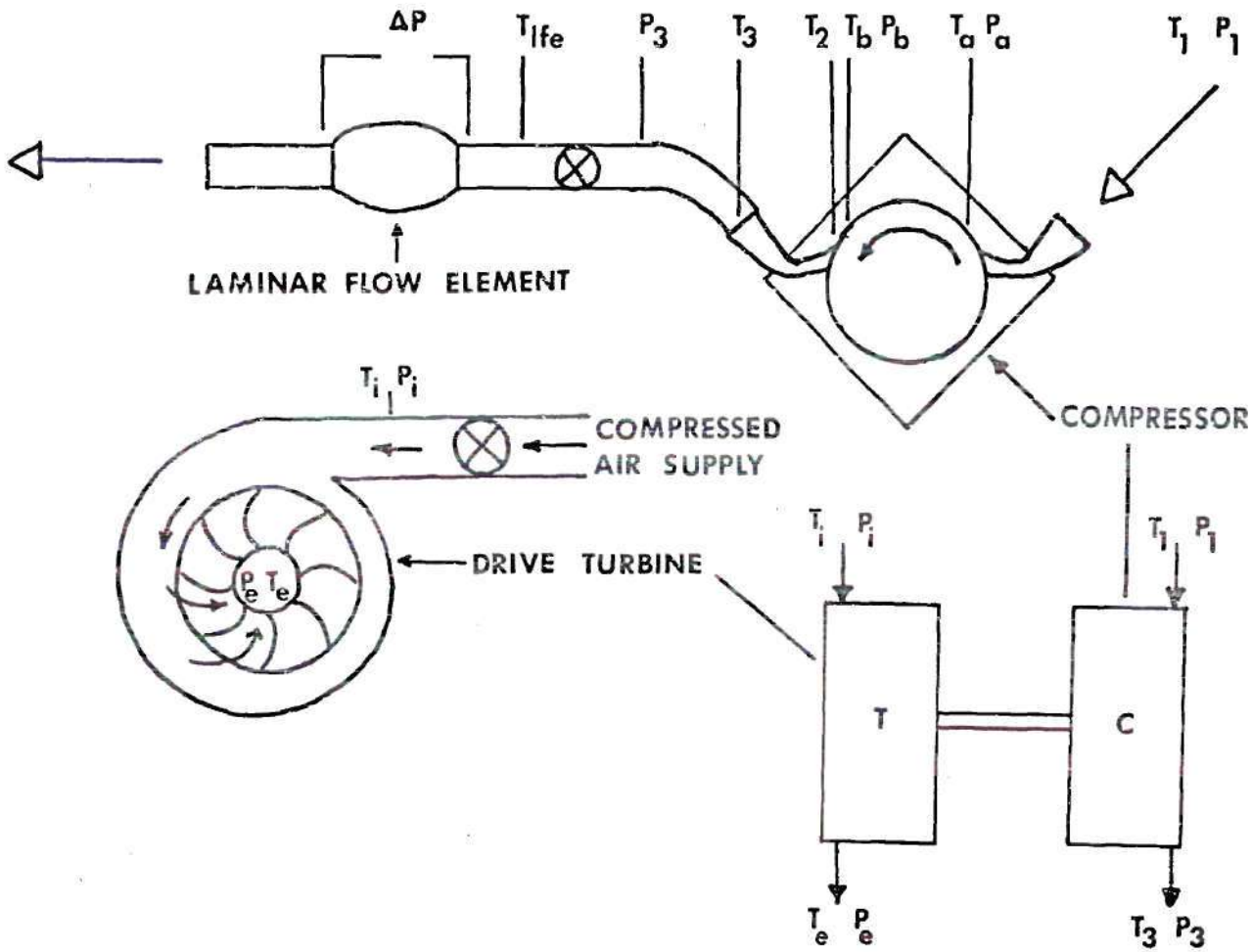

Figure 4. Experimenal Apparatus.

2-2. Measurements

The ambient conditions, P_1 and T_1, were measured using a mercury barometer and a thermometer. The angular velocity of the compressor wheel was measured by a magnetic pick-up and an electric counter. The turbine inlet pressure P_i, and the compressor pressures P_a and P_b were measured using standard pressure gauges. The turbine exit pressure P_e, and the diffuser exit pressure P_3, were determined using mercury manometers. The volumetric flow rate of the compressed air supply to the drive turbine was calculated from the pressure drop across an orifice plate in the feed line. This pressure drop was measured using a water manometer. A sample calculation for determining this flow rate is contained in Appendix C-1. The volumetric flow rate of the compressor flow was calculated from the pressure drop across a laminar flow element (Meriam, model 50MC2-2P). This flow was then referred to standard temperature and pressure by means of the Meriam temperature correction curve and pressure correction chart shown in Figure 20 and Table 6, respectively. The temperatures T_a, T_b, T_{1fe}, T_i, and T_e were measured using copper vs. constantan thermocouples.

All of the data obtained in the investigation is tabulated and included in Appendix A.

2-3. Procedure

Teflon seal teeth were initially tested in the compressor. They were made according to the following procedure.

1. A cutter was manufactured with a thickness equal to the thickness of the thinnest wheel disc (0.052 in.). See Figure 21 in the Appendix for the detailed wheel measurements.

2. The cutter was mounted on a milling machine and eleven cuts were made in a two-inch cube of teflon according to the measurements of the wheel.

3. The teflon was then sliced perpendicular to the cuts to make multiple sets of seal teeth. The teeth were then fastened to the aluminum blocks with screws.

4. The titanium wheel was then mounted on a lathe and turned at approximately 1000 rpm while the seal teeth were forced very slowly into the wheel grooves. This step resulted in the best possible mating of the teeth and the wheel.

5. The tips of the seal teeth were ground to a point and the excess teflon was trimmed from the sides.

Inconel X-750 seal teeth were constructed after the teflon seal teeth had been tested and found unsuitable. The inconel seal teeth were made in a similar manner as the teflon teeth according to the following steps.

1. Four sheets of inconel, 1 3/8" x 1½" x 0.015", were sandwiched and clamped between two strips of brass to give support. Cuts were then made in the brass and inconel according to the wheel measurements. The same cutter was used for the inconel as was used for the teflon.

2. The sets of teeth were then mounted on the aluminum seal blocks and trimmed to the appropriate width. A point file was used to make adjustments to the width of individual teeth.

3. Once the teeth would fit into the grooves of the wheel, the wheel and seals were installed in the compressor. The wheel was then

turned very slowly by hand to wear in the seal teeth.

Data were collected for each experimental run according to the following procedure.

1. The compressor was started and run at 7000 rpm while the casing was being bolted into place. This was done very slowly to allow the seals to be properly seated. This was necessary because the casing gasket caused slight movement of the seal blocks as the casing bolts were tightened.

2. The gate valve in the compressor exhaust line was set to the wide-open position and the speed of the compressor was then set to the desired level by adjustment of the gate valve in the compressed air feed line.

3. Once the desired speed was achieved, the compressor was allowed to stabilize. Then the temperatures and pressures were recorded at each of the compressor exhaust gate valve settings in order from wide-open to shut-off. Adjustments to the compressor speed were made when necessary to maintain a constant speed at each setting of the compressor exhaust gate valve.

4. At the completion of the data collection at a given speed, the compressor exhaust gate valve was returned to the wide-open position. The compressor speed was then increased to the next level and the above procedure was repeated.

The teflon seals and one set of inconel seals sustained heavy damage when the compressor was operated at the shut-off position. Therefore, the above procedure was modified to exclude operation at the shut-off position when the data for inconel seals in this report were collected.

CHAPTER III

RESULTS

3-1. The Experimental Limit

Initially the test program called for each type of seal to be tested over the same range of operation as the graphite seal design of Dusadeenoad (7). However, both the teflon and inconel seals failed to some degree before a speed of 42,000 rpm was reached.

In the case of the teflon seals, operation was limited to 35,000 rpm due to evidence that the volume flow rate was being severely restricted. It was determined that the teflon dust created by the disintegration of the seal teeth was clogging the laminar flow element. The pressure rise versus flow rate characteristic curves for the compressor with the teflon seal teeth installed are shown in Figure 5.

By observing Figure 5, one can see that the seal teeth began disintegrating between the runs at 15,000 rpm and 20,000 rpm. This is illustrated by the smaller increment of flow than for the increase of speed from 10,000 rpm to 15,000 rpm. Also, it appears from the curves in Figure 5 that all of the teflon teeth were finally destroyed during the run at 30,000 rpm.

In the case of the inconel seals, data were obtained at speeds up to 42,000 rpm. However, during operating it became evident that some of the seal teeth were missing, and that operation at greater speeds would be fruitless. The pressure rise versus volume flow

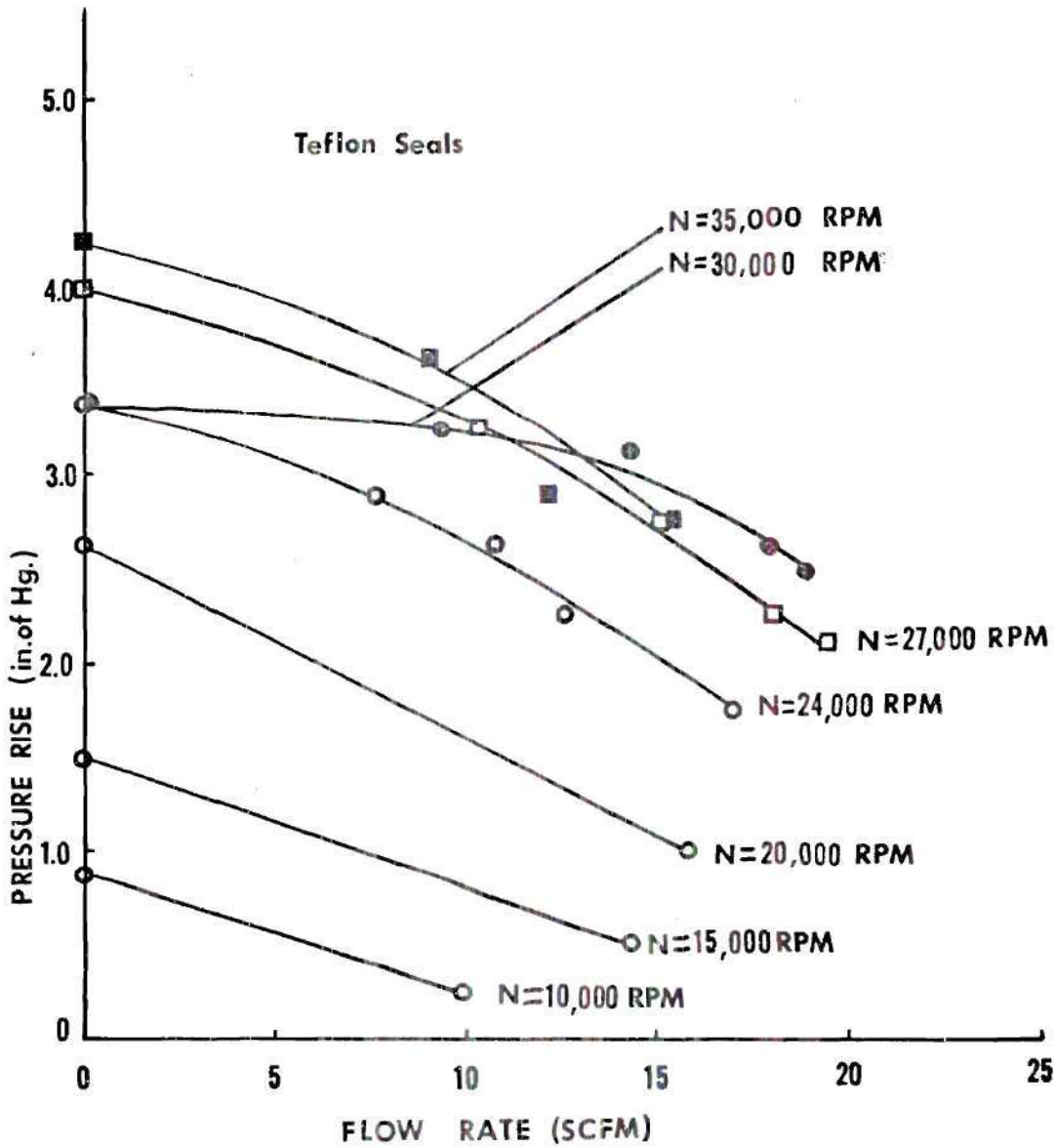

Figure 5. Pressure Rise vs. Flow Rate — Teflon Seals.

rate characteristic curves for the compressor with inconel seal teeth installed are shown in Figure 6.

In this figure, one can see that the teeth began to wear between the runs at 20,000 rpm and 24,000 rpm. Teeth appear to have broken off at speeds of 30,000 rpm, 40,000 rpm, and 42,000 rpm.

3-2. Comparison Between Experimental Curves and Theoretical Curves

Theoretical pressure rise versus volume flow rate curves for speeds from 15,000 rpm to 70,000 rpm were developed by Traviss (6) and published by Dusadeenoad (7) and these curves are shown in Figure 7. A comparison of the theoretical curves and Figures 5 and 6 clearly indicate poor results from both the teflon and inconel seals. For example, at 15,000 rpm the theoretical curve shows a pressure rise of approximately 3.3 inches of mercury at a flow rate of 10 scfm. The compressor with teflon seals installed obtained a pressure rise of 0.8 inches of mercury at the same speed and volume flow rate. With inconel seals installed, the pressure rise was 0.85 inches of mercury. The theoretical maximum flow rate at 15,000 rpm predicted by Traviss and contained in the report by Dusadeenoad was approximately 27 scfm. The maximum flow rate obtained at that speed with the teflon seals was 14.3 scfm. With the inconel seals installed, the maximum flow rate was 15.9 scfm at 15,000 rpm. The differences between theoretical values and experimental results becomes greater as the speed of the compressor is increased.

Tables 1 and 2 contain the experimental data used to produce the pressure rise versus volume flow rate curves.

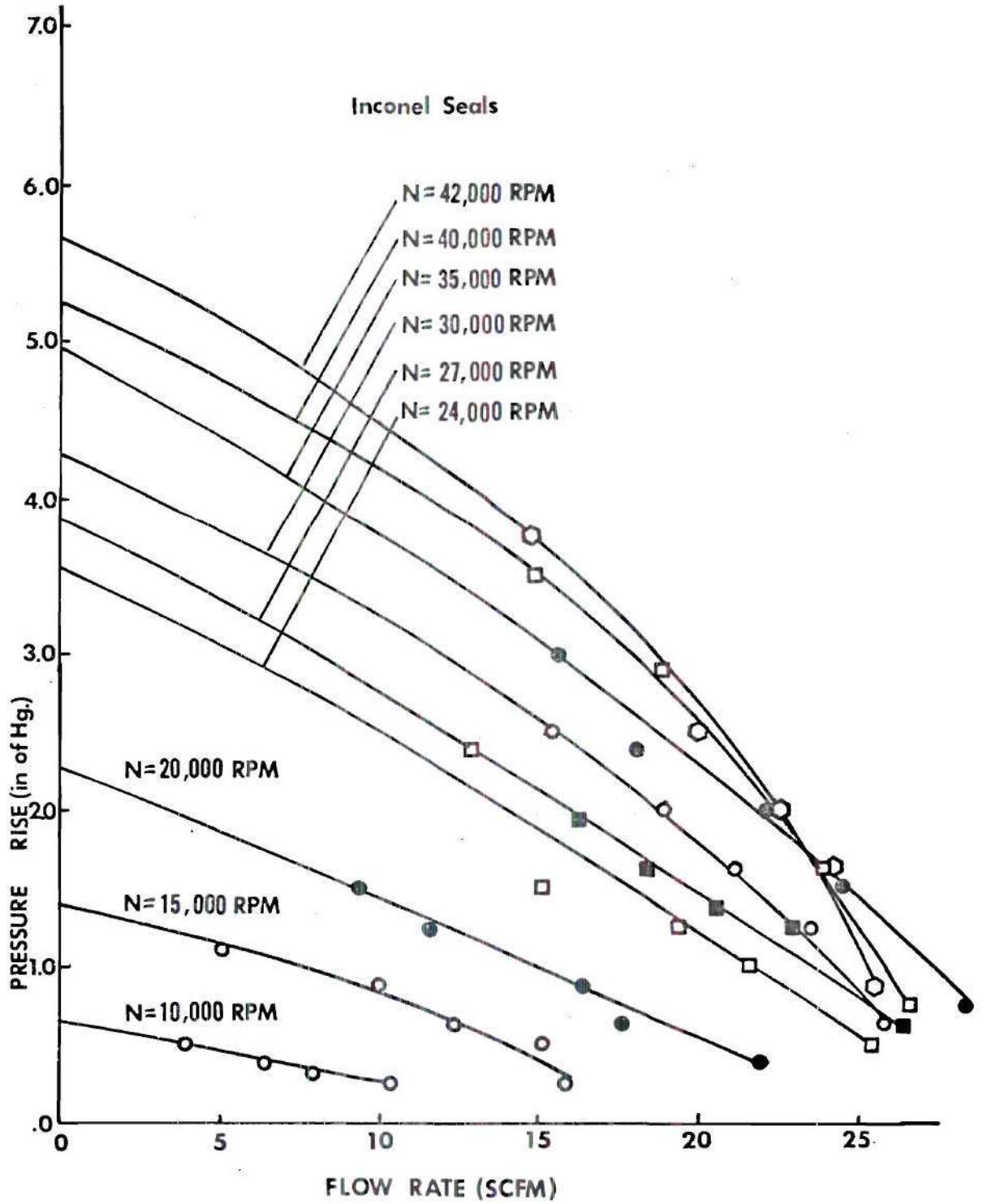

Figure 6. Pressure Rise vs. Flow Rate—Inconel Seals.

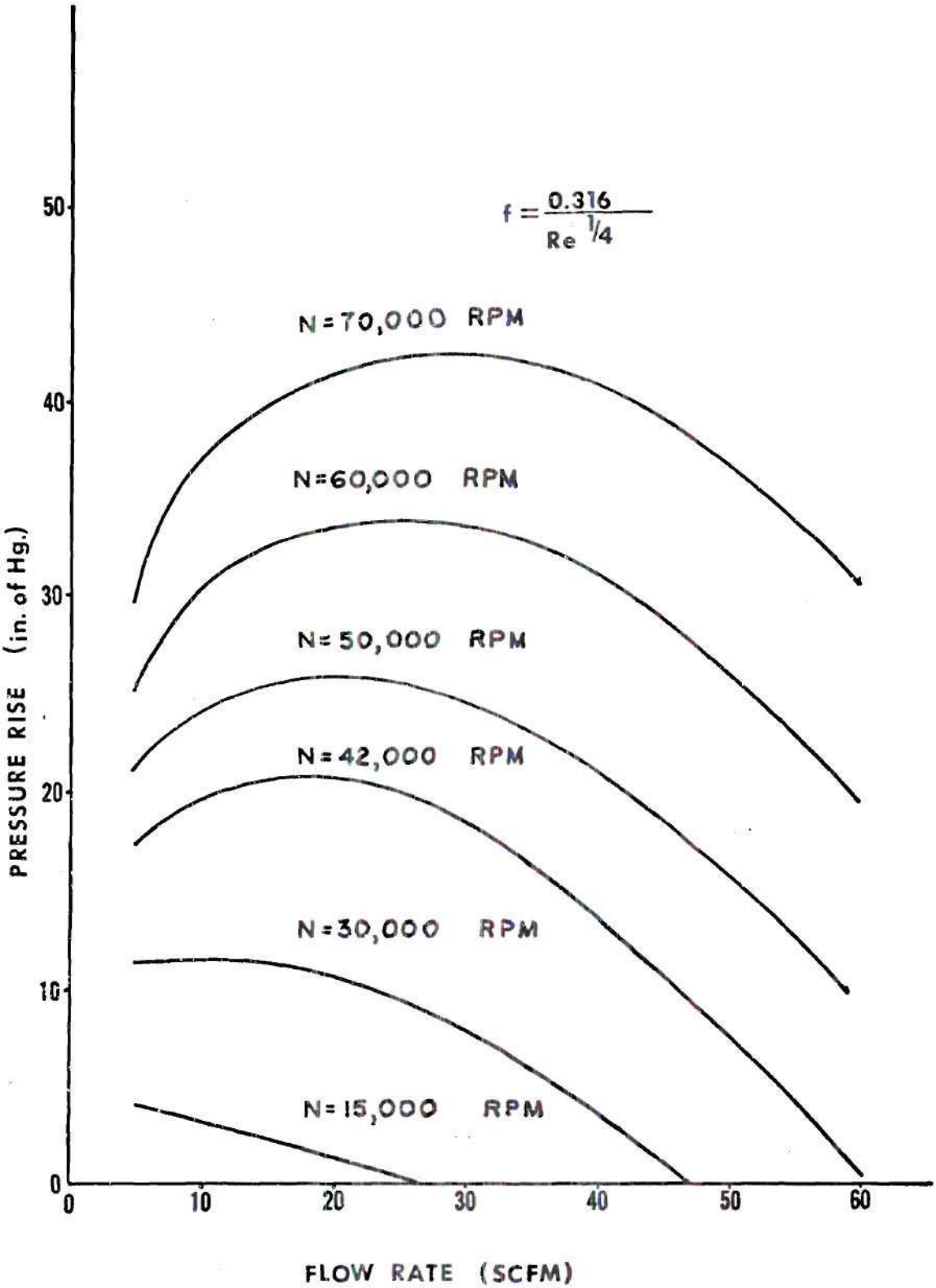

Figure 7. Theoretical Pressure Rise vs. Flow Rate (7).

3-3. Adiabatic Compression Efficiency

Compression efficiency is defined generally as the ratio of work required for the reversible process to the work required for the actual process, both for the same pressure ratio (9). In most turbomachinery, the actual process is essentially adiabatic. For purposes of this investigation, the reversible process was also assumed adiabatic and therefore isentropic. Thus, the adiabatic compression efficiency is defined as

$$\eta_c = \frac{\text{Work assuming isentropic compression}}{\text{Work required for the actual compression}} = \frac{c_p \left(T_{0_3} - T_{0_1} \right)}{c_p \left(T_{0_3'} - T_{0_1} \right)}$$

For this study, efficiencies were based on total (stagnation) values of temperatures at the compressor inlet and exhaust. Stagnation values include kinetic energy terms and are represented by a "0" subscript. Therefore,

$$T_0 = T + \frac{V^2}{2 g_c \, c_p \, J}$$

Sample calculations for the adiabatic compression efficiency are shown in Appendix C-2.

Figure 8 shows the adiabatic compression efficiencies obtained for the compressor with inconel seals installed, and Figure 9 shows the efficiencies obtained with the teflon seals installed. These results can be compared to the results obtained by Dusadeenoad, which are contained in Figure 10. A comparison indicates that the current seal design, using either teflon or inconel seal teeth, resulted in

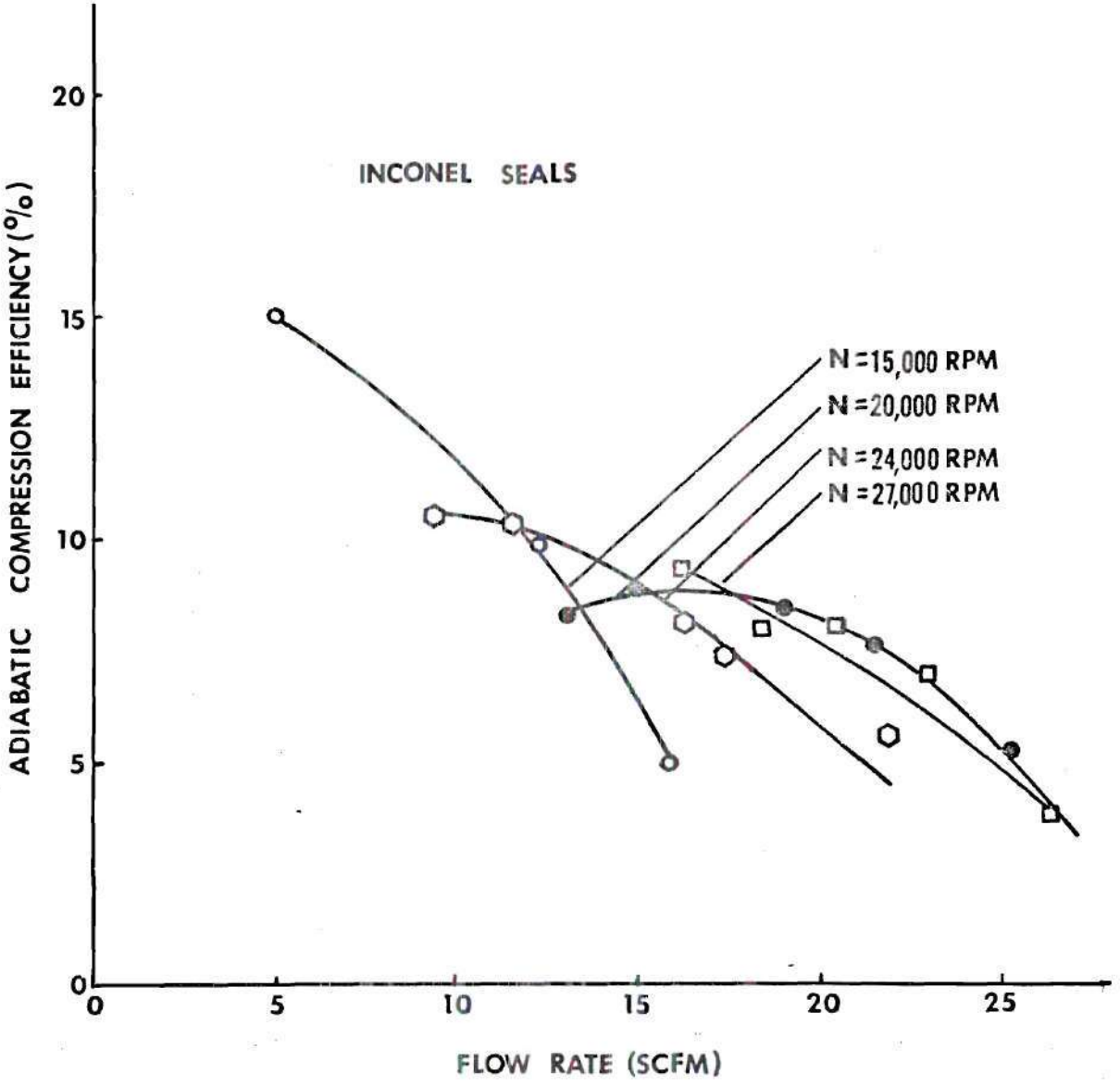

Figure 8. Adiabatic Compression Efficiency.

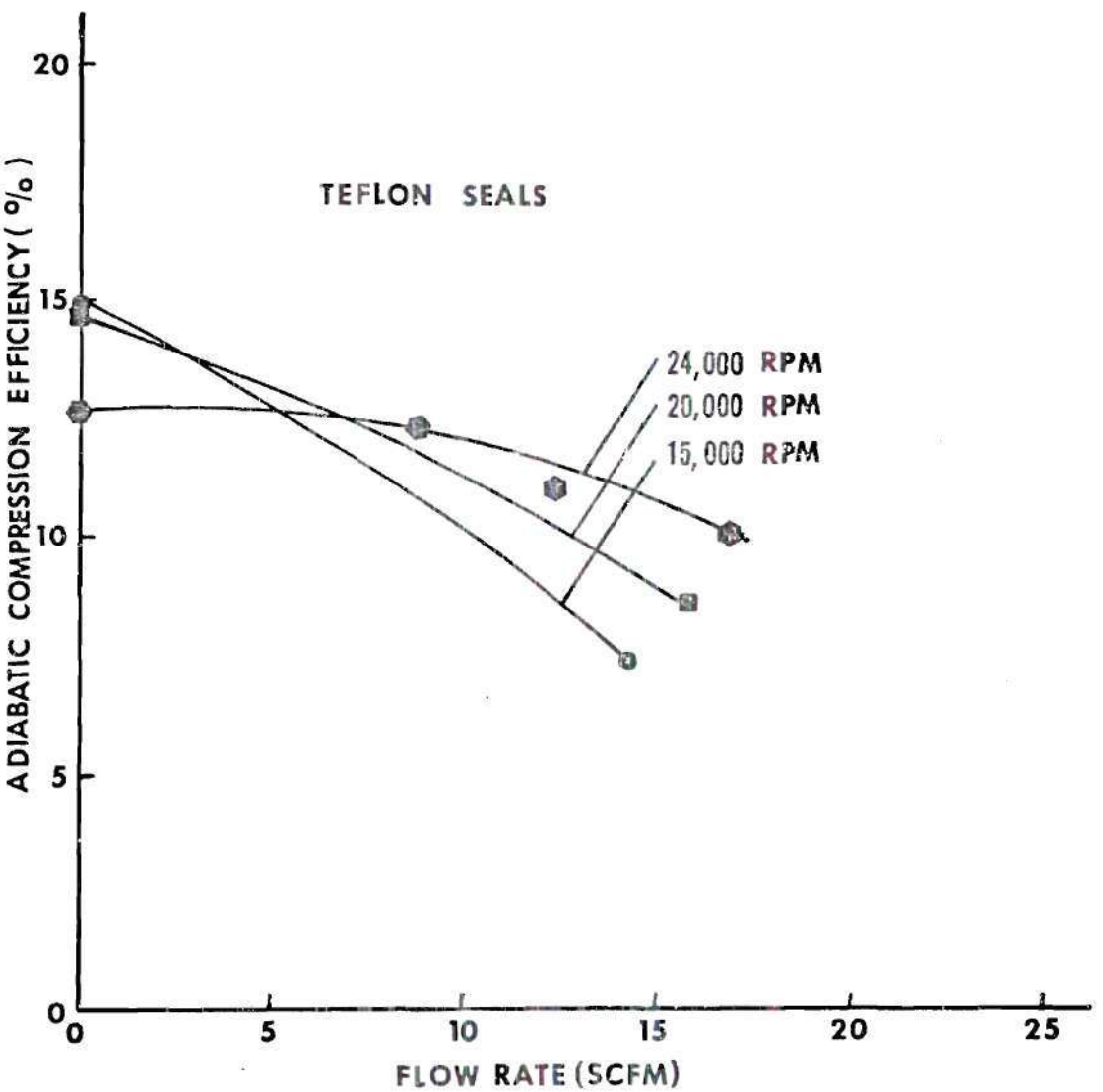

Figure 9. Adiabatic Compression Efficiency.

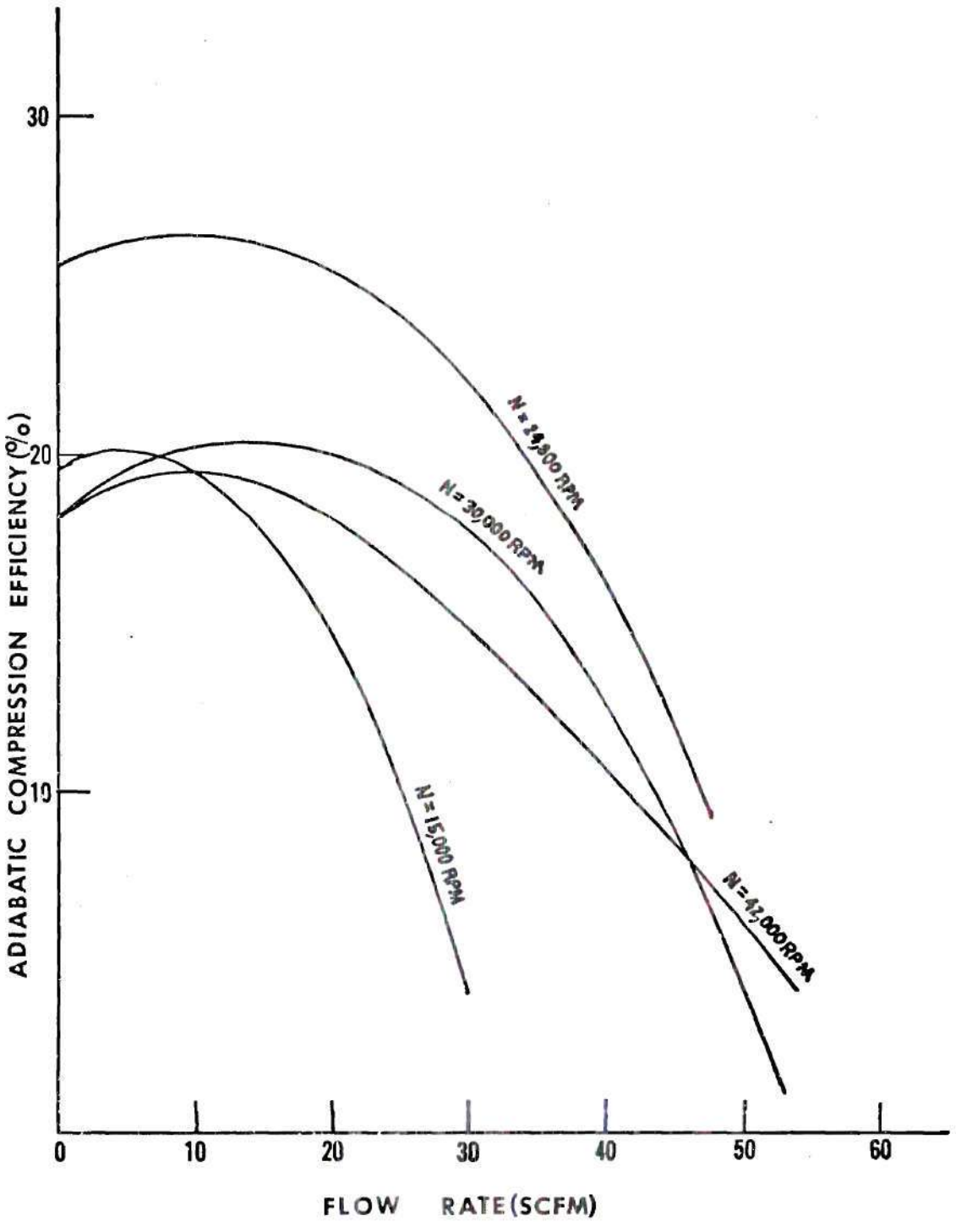

Figure 10. Adiabatic Compression Efficiency—Graphite Seals(7).

significantly lower adiabatic compression efficiencies at all compressor speeds. The large decline in the efficiency as the speed was increased is directly related to deterioration of the seal teeth. As a result of this deterioration, the adiabatic compression efficiencies are shown only up to 24,000 rpm for teflon seals and up to 27,000 rpm for inconel seals.

3-4. Temperature Profile

Figures 11 and 12 show the curves of the compressor temperatures T_a, T_b, and T_{1fe} versus volume flow rate for the inconel seals at speeds of 24,000 rpm and 30,000 rpm respectively. Figures 13 and 14 show the same curves for the teflon seals. Comparison of these curves with the corresponding results of Dusadeenoad, contained in Figures 15 and 16, indicates slightly higher temperatures at a given flow rate were obtained with the graphite seals. When making this comparison, one should assume that most of the teflon teeth had been worn away by the time a speed of 24,000 rpm was reached. Also note that T_a corresponds to Dusadeenoad's T_1 and T_b corresponds to T_2.

3-5. Turbine and Compressor Power Losses

The power losses attributed to the turbine bearings and glands, compressor wheel windage and disc friction, and seal drag were experimentally determined for the compressor with inconel seals installed.

In order to determine the turbine bearing and gland losses, a test run was made with a cylindrical spacer substituted for the compressor wheel. The power absorbed in the turbine rotor for this run was then subtracted from the power absorbed during the run with the

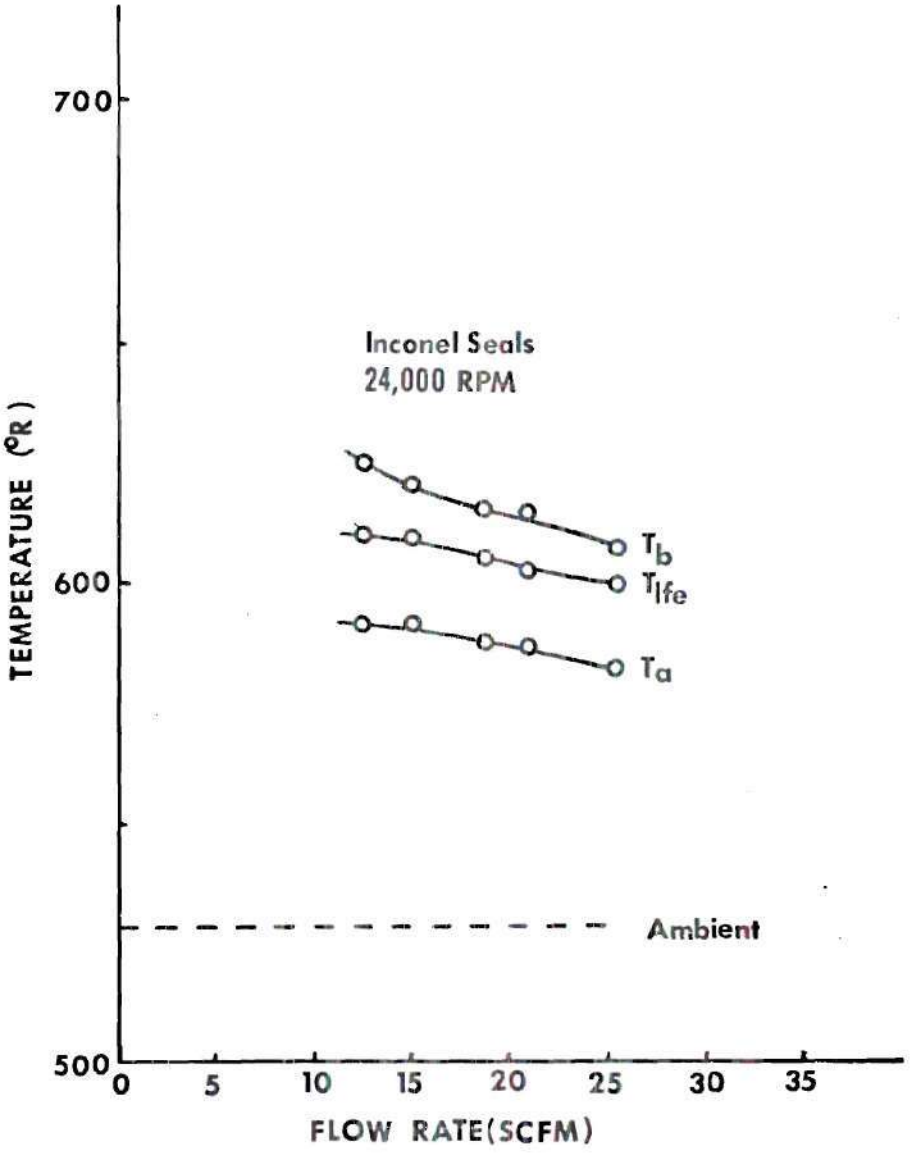

Figure 11. Temperature Profile.

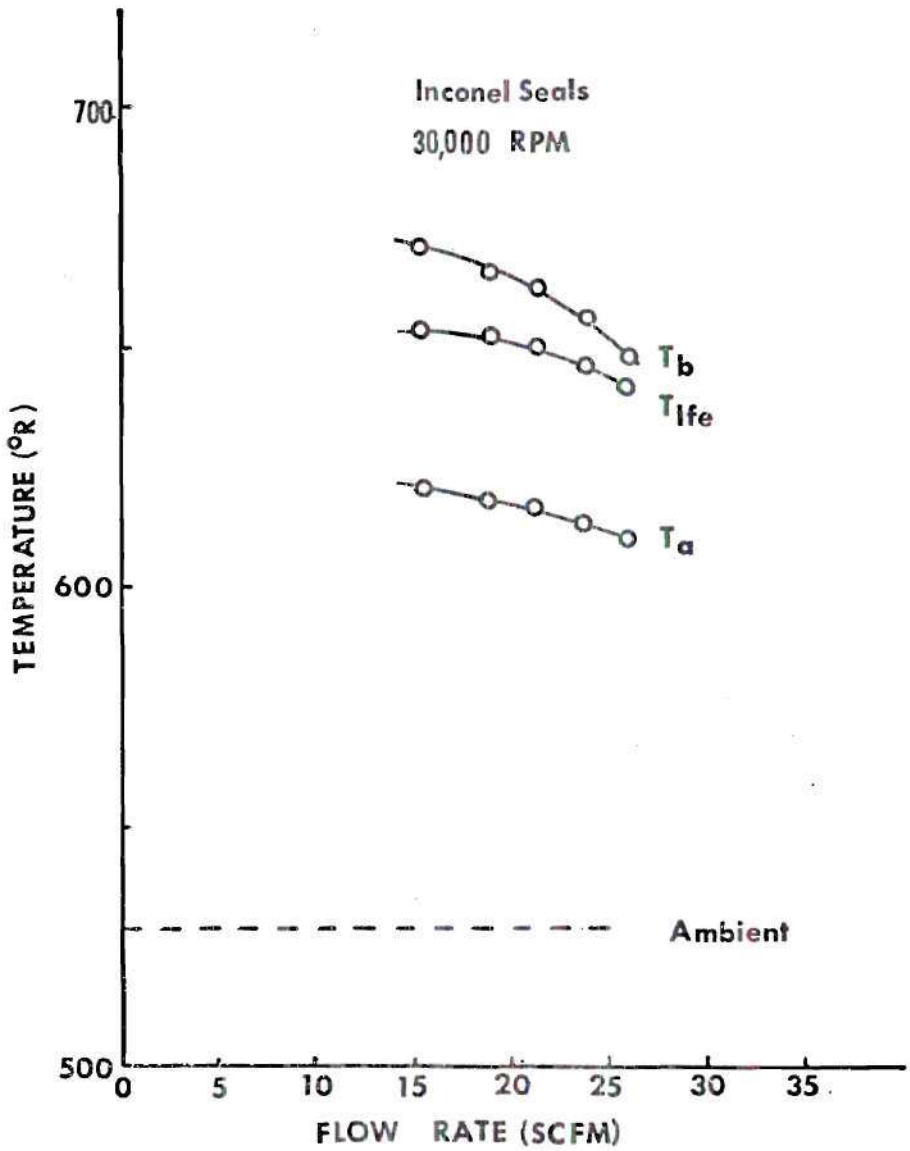

Figure 12. Temperature Profile.

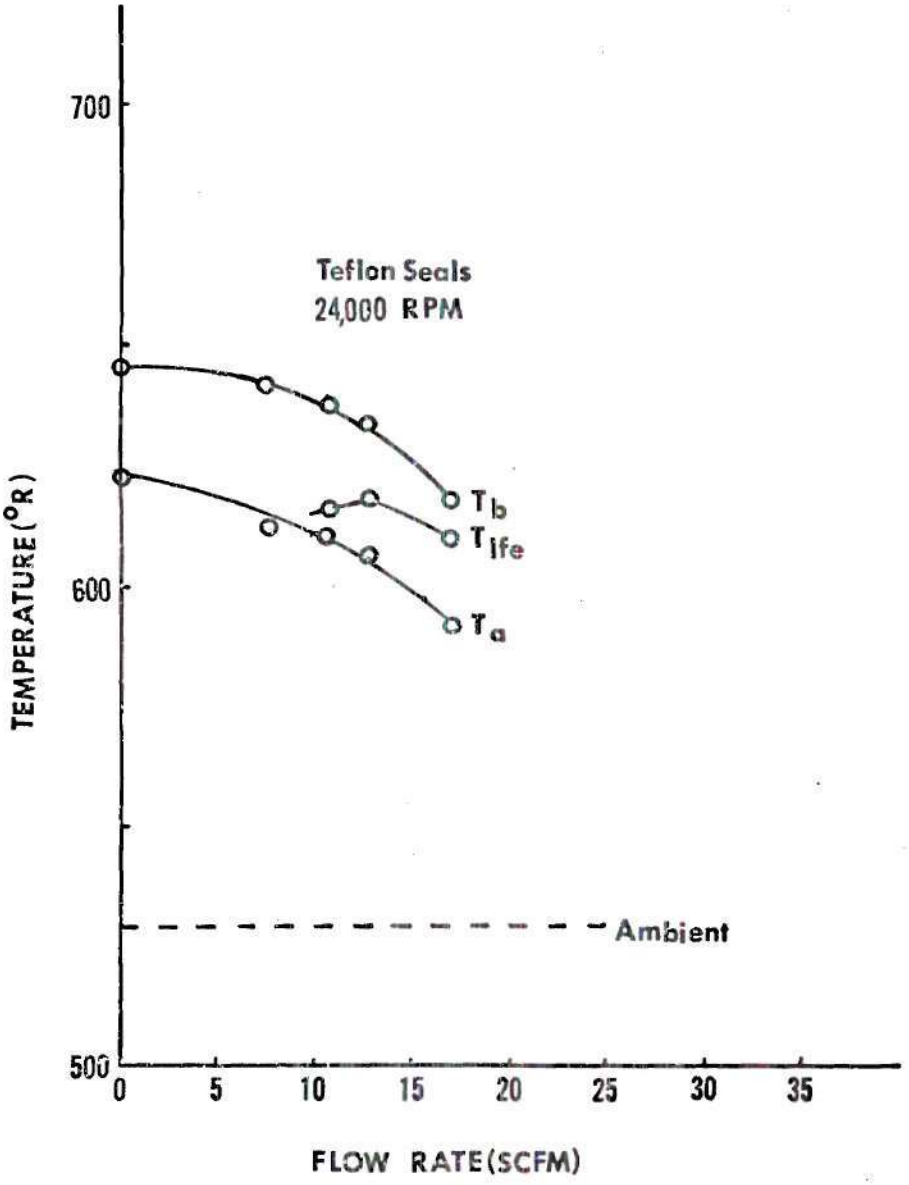

Figure 13. Temperature Profile.

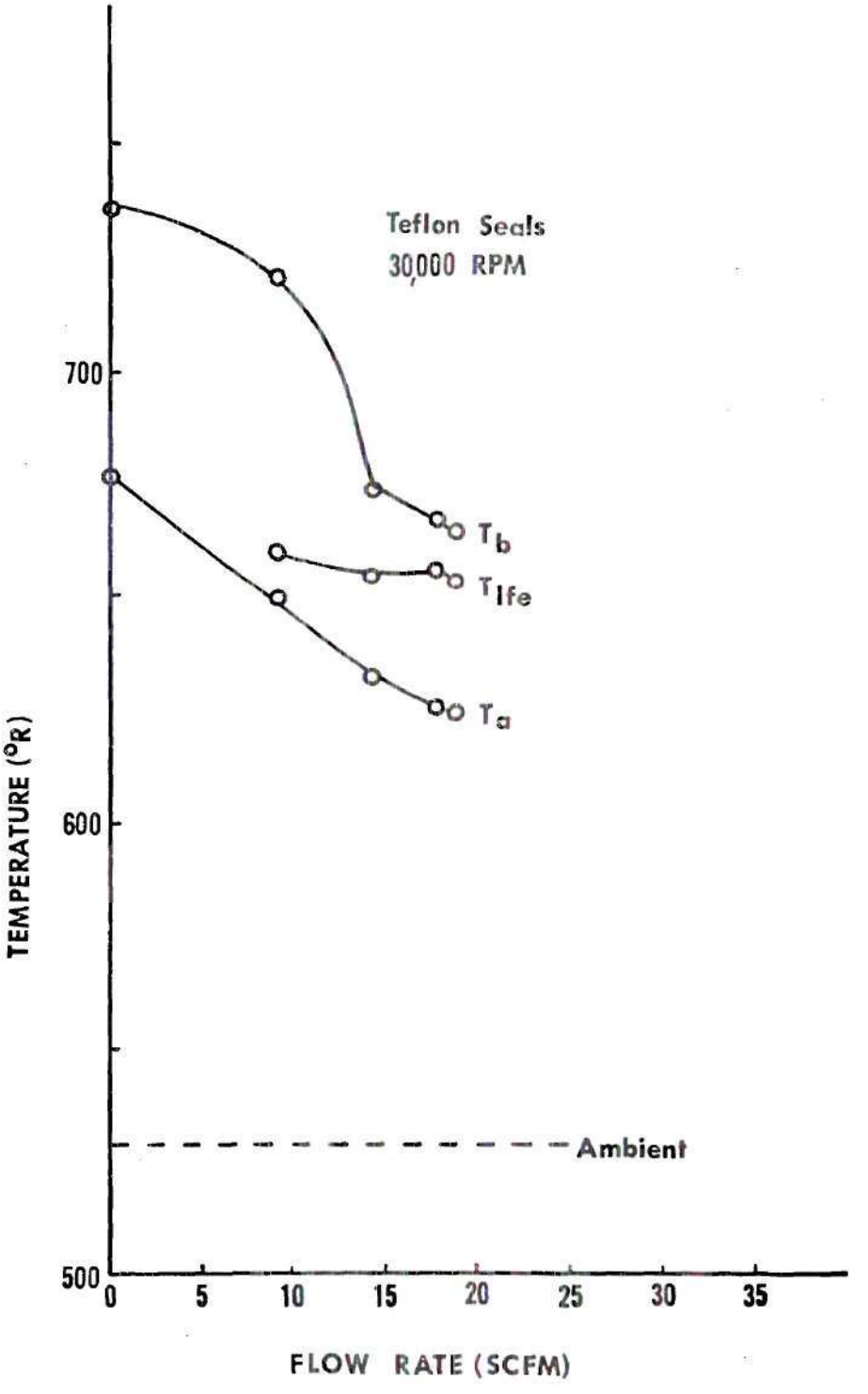

Figure 14. Temperature Profile.

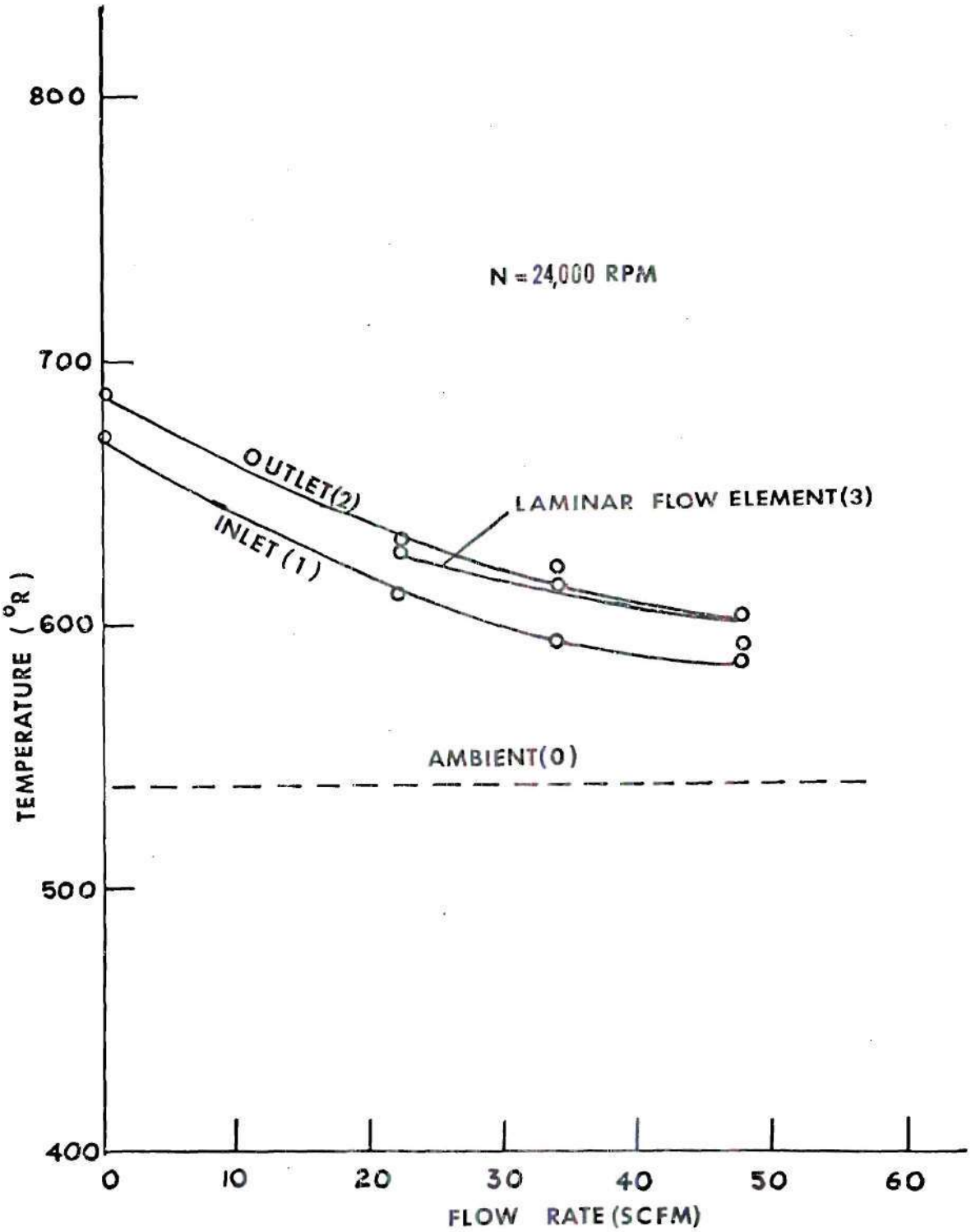

Figure 15. Temperature Profile — Graphite Seals(7).

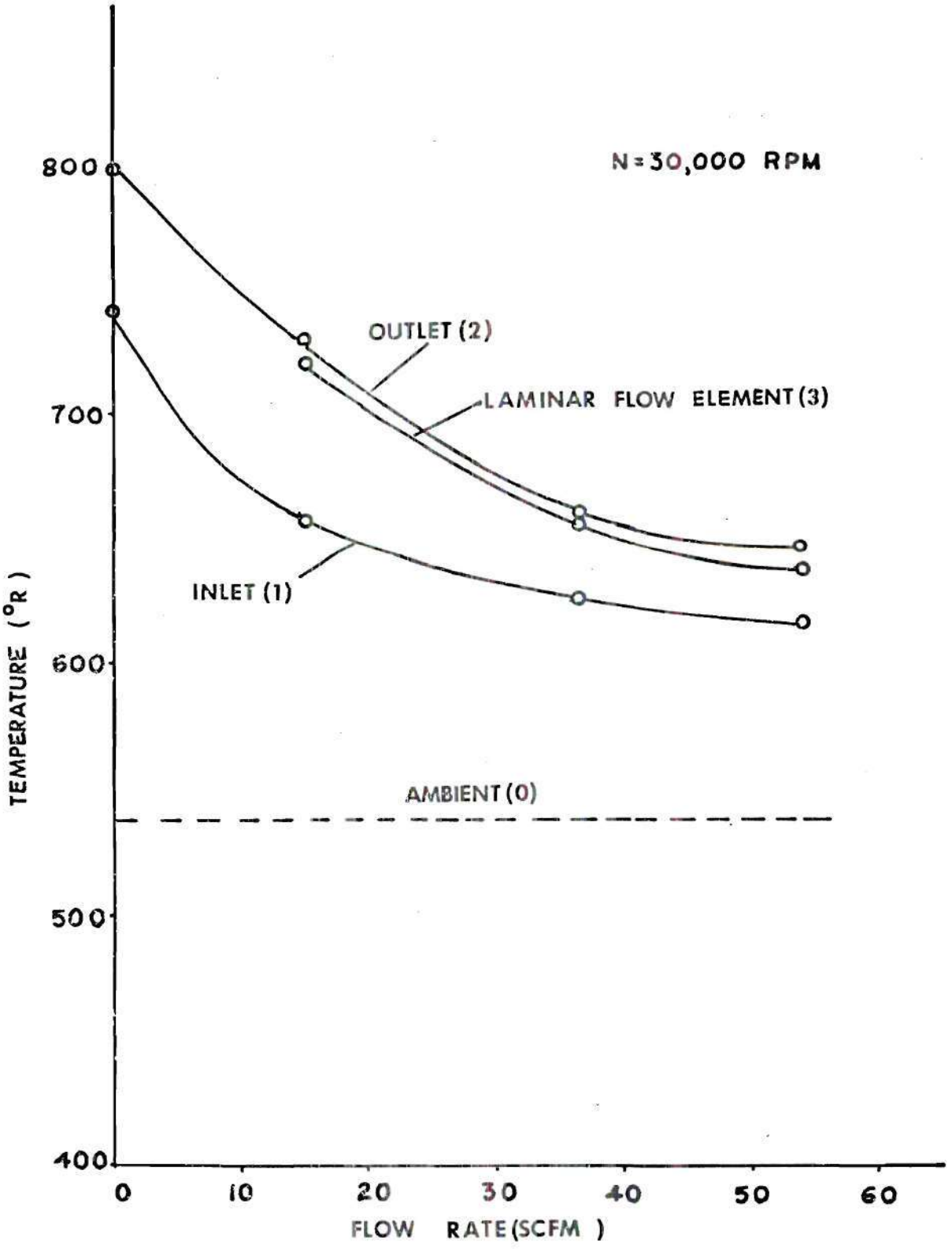

Figure 16. Temperature Profile—Graphite Seals(7).

wheel and seals installed in the compressor. This quantity represented the combined power loss of the work of compression, seal drag, windage, and disc friction. The combined seal drag and work of compression power loss was determined by subtracting the power absorbed in the turbine rotor during a run with no seals installed in the compressor from the power absorbed in the turbine rotor with the seals installed. The amount of power allocated to the compression process was calculated using an average friction factor. Figure 17 shows the various power losses versus rpm for a constant system resistance. This system resistance was chosen at a mid-flow setting of the compressor exhaust valve. Sample calculations to support the curves in Figure 17 are contained in Appendix C-3. These power losses are tabulated in Table 5.

The results shown in Figure 17 indicate that only a very small percentage of the power absorbed in the turbine rotor was actually applied to the compression process.

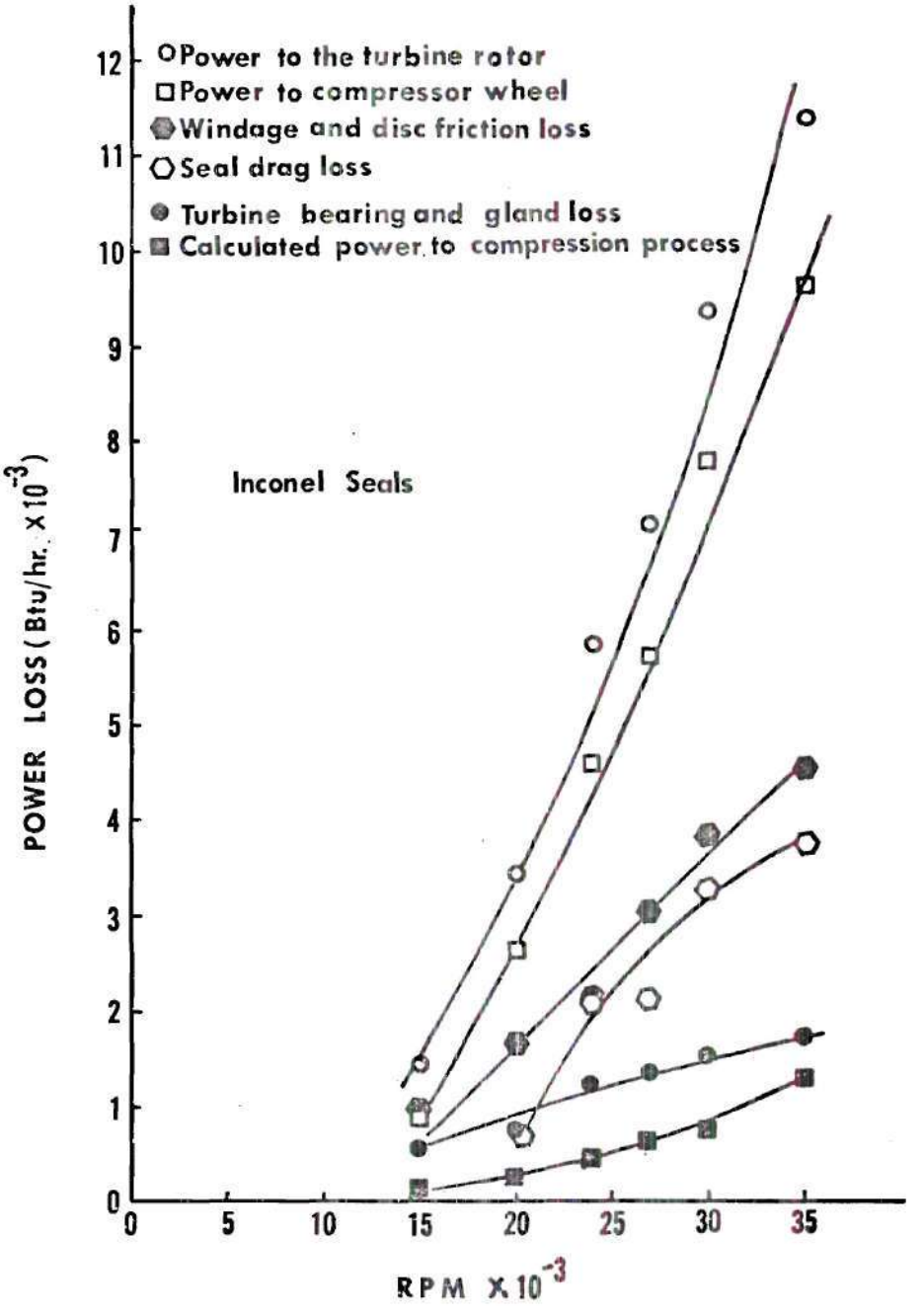

Figure 17. Power Losses.

CHAPTER IV

DISCUSSION OF RESULTS

4-1. General

The author had two main objectives to accomplish in this experimental investigation. The first was to develop a durable, efficient seal design which had a significantly reduced wearing surface vis-a-vis the wheel as compared to the design used by Dusadeenoad. The durability of the design depended on the material properties as well as the structural characteristics. Previous attempts, as reported in Chapter I, had failed to produce a suitable design.

As a result of this investigation, teflon can be eliminated from the list of possible seal materials. On the other hand, inconel X-750 warrants further investigation. It is believed that the failures incurred with the seal teeth made of this material were due to structural weaknesses of the design rather than a lack of sufficient material properties.

The second major objective of this investigation was to determine the efficiency of this compressor. The calculated adiabatic efficiencies are only marginally useful due to the poor seal performance and the large mechanical power losses in the compressor. In short, reasonable adiabatic compression efficiencies, which might compare favorably with efficiencies of conventional compressors, cannot be achieved until the first objective is successfully completed.

4-2. Evaluation of the Seal Configuration

To date, the most successful seal configuration has been the one used by Dusadeenoad (7). However, the temperature profiles reported in his results indicated exit temperatures (T_{0_3}') much higher than predicted values at the higher flow rates. It was believed that these high temperatures could be significantly reduced by a drastic reduction of the seal surface area vis-a-vis the wheel. A decrease in the exit temperature would result in a corresponding increase in the adiabatic compression efficiency.

As indicated in Section 3-4, the exit temperature was not significantly reduced as a result of the reduced seal area, or by a change in the seal material. Therefore, the exit temperature in this compressor is not a strong function of these variables, as had been previously believed.

The results of this investigation indicate that the drastic area reduction in the current seal design caused two detrimental effects in the seal performance. First, these seals simply did not form an effective face seal with the sides of the wheel discs. The resulting excessive leakage caused a reduction in pressure rise, flow rate, and adiabatic compression efficiency as compared to the results of Dusadeenoad. Second, this reduction of surface area diminished the strength and rigidity of the seal teeth, thus subjecting them to excessive wear and breakage.

In the case of the teflon seal teeth, the inherent flexibility of the material, coupled with the lack of structural rigidity, allowed

the seal teeth to flutter as the air passed by them at high velocities. This resulted in continuous wear and eventual total disintegration of the seal teeth as shown in Figure 18a.

The seal teeth made of inconel possessed the material strength to resist the excessive flutter, and as a result, they sustained very little wear after the initial break-in period. The damage to the inconel teeth was sustained when the teeth were flexed downward onto the wheel hub by the higher pressure forces incurred at increased speeds and low flow rates. When contact was made with the wheel, some of the teeth were ripped off by the wheel. The results of this breakage are shown in Figure 18b. In the photograph, the seal teeth on the left were installed on the exhaust side where the higher pressures existed.

The fact that the seals were forced down onto the wheel probably accounts for the very high seal drag power loss shown in Figure 17.

If the inconel seal teeth had been of a more rigid construction, it is believed that the breakage and seal drag would have been minimized.

One positive aspect of this seal configuration was the ability to interchange the sets of seal teeth. This allowed the testing of several types of material without the additional investment of time and money in the manufacture of new seal blocks.

4-3. Efficiency

When discussing the efficiency of a turbomachine, one must

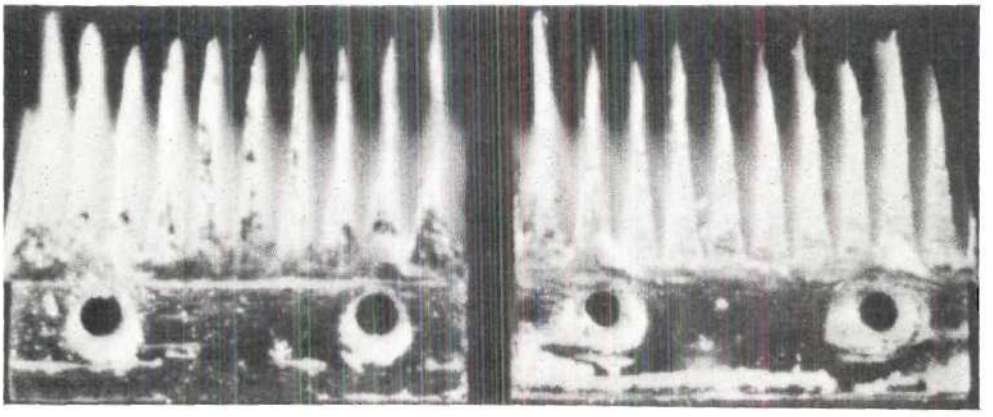

a

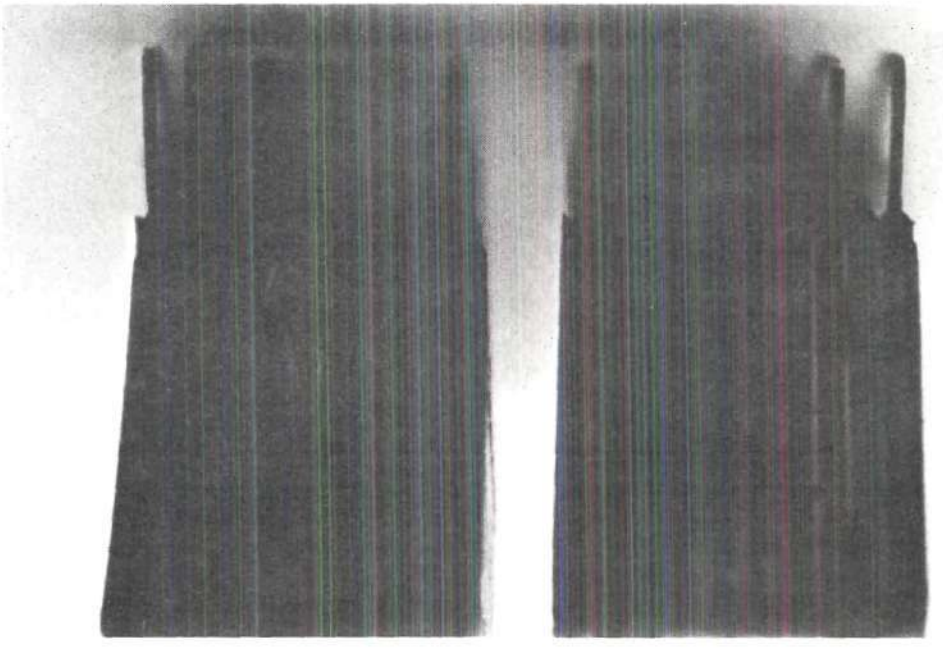

b

Figure 18. Worn Seals.

carefully define terms, and insure that the actual machine performance reasonably conforms to the assumptions used to derive the equation for efficiency. The compression process in most conventional compressors is nearly adiabatic. Therefore the adiabatic compression efficiency, as defined in Section 3-3, is a valid measure of the performance of this type of compressor.

However, the actual compression process in the particular compressor examined in this study was a drastic departure from an adiabatic process. This was caused by several features peculiar to this experimental apparatus. First, this compressor incurs very high mechanical power losses as illustrated in Figure 17. The mechanical efficiency (η_m) of a compressor is defined as the ratio of rotor horsepower (power to actual compression process) to shaft horsepower(11). As an example of the mechanical efficiency of this compressor, refer to Figure 17 and Table 5. Choosing the appropriate values at 24,000 rpm we calculate

$$\eta_m = \frac{405 \text{ BTU/hr}}{4612 \text{ BUT/hr}} = 8.75 \text{ per cent}$$

The mechanical efficiencies of most compressors is in the range of 97 per cent to 99.5 per cent when based on rated-load capacity (11). Therefore, the dissipation of mechanical energy into thermal energy was unusually great in this machine. This generation of thermal energy probably made a significant contribution to the large stagnation temperature difference, $(T_{0_3'} - T_{0_1})$, in the denominator of the adiabatic compression efficiency definition.

Another factor which seemed to increase the actual stagnation temperature difference in this particular compressor was the apparent heat transfer from the shaft bearing and bearing oil. This bearing is located immediately adjacent to the compressor rear casing. Only limited data was taken concerning the oil temperature, and this is contained in Table 4. When the compressor was run with a spacer substituted for the wheel, the temperatures T_a and T_b were still very high. Since there could be no disc friction or seal drag without the wheel, the only possible source of the high temperatures had to be the oil and the bearing. This is substantiated by the fact that the oil temperature was measured at a point after the oil had been cooled.

In order to present a useful efficiency rating for this compressor under the circumstances, an expression for internal efficiency should be considered. The internal efficiency is defined as

$$\eta_{ic} = \frac{\text{isentropic work}}{\text{actual work on the gas}} \qquad (11)$$

Figure 19 shows curves of η_{ic} versus flow rate for speeds of 15,000 rpm, 20,000 rpm, and 24,000 rpm. The sample calculation for the internal efficiency is contained in Appendix C-4.

4-4. The Tapered Disc Profile

The authors of previous investigations (5,6) had recommended that the edges of the wheel discs be tapered rather than flat. The effect would be to reduce aerodynamic losses and increase the compressor efficiency.

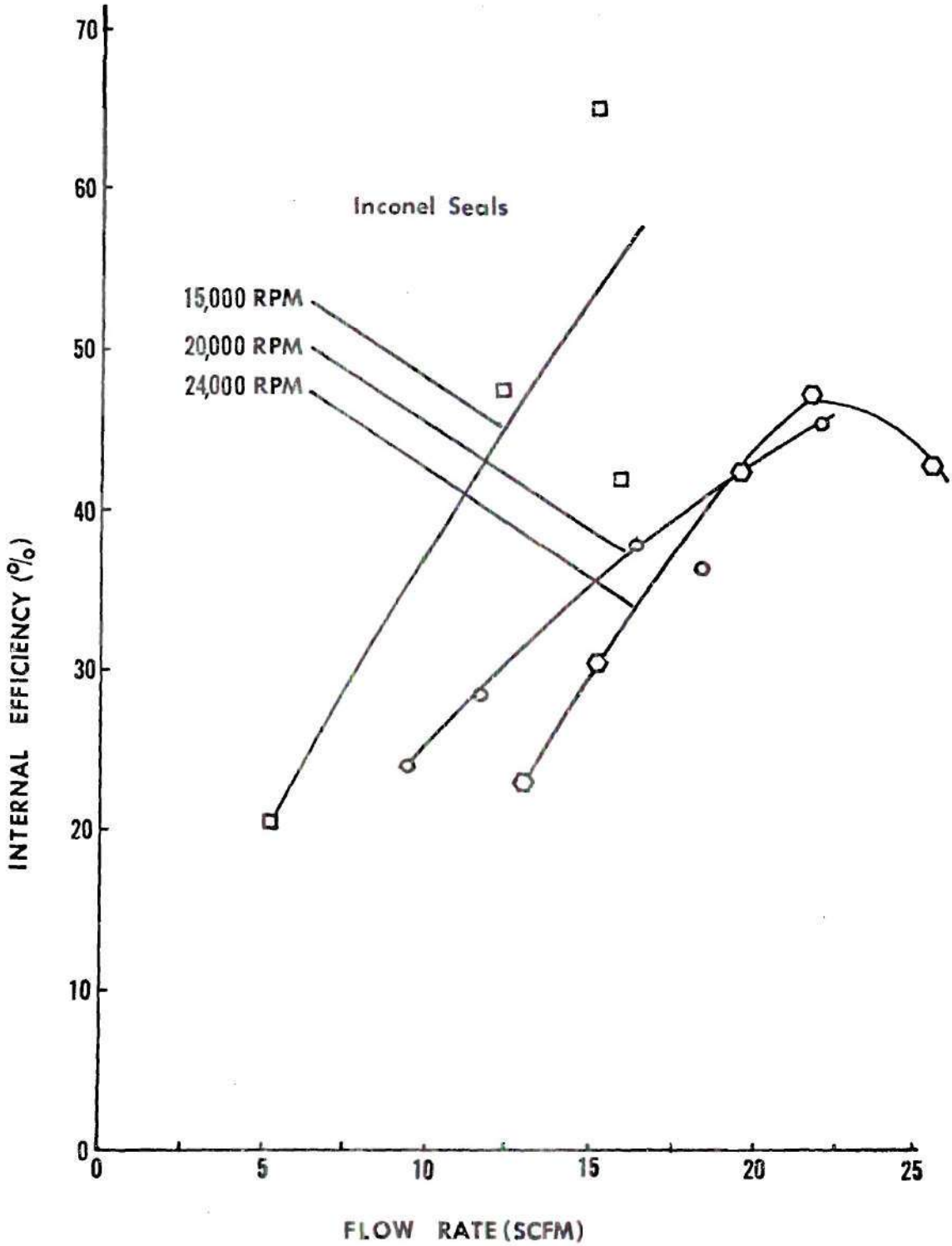

Figure 19. Internal Efficiency.

Based on the results of this investigation, there is no way to evaluate the actual effect of the tapered discs other than to say that it did facilitate the wearing in of the teflon seal teeth. The increased leakage which resulted from the new seal design more than off-set any gain in efficiency due to the tapered disc tips.

4-5. The Effect of Poor Wheel Construction

When evaluating the results of this investigation, the detrimental effects of several of the features of the wheel construction cannot be minimized. First of all, the wheel discs are not exactly perpendicular to the shaft. Second, the discs are not all of the same thickness. They vary from 0.052 inches to 0.083 inches thick. Third, when rotating, the wheel has an axial run-out of 0.006 inches.

All of the above features made the design and construction of an efficient, durable seal very difficult.

CHAPTER V

CONCLUSIONS AND RECOMMENDATIONS

The results obtained in this investigation lead to the following conclusions:

1. The seal design tested in this investigation did not provide an adequate face seal with the sides of the wheel discs.

2. The seal design was not rigid enough to maintain the proper configuration with respect to the wheel at the higher exhaust pressures.

3. Teflon is not a suitable seal material to satisfy the requirements of this compressor.

4. Inconel X-750 should be considered as a potential seal material for future seal design for this type of compressor.

5. The "detachable-seal-teeth" feature of the investigated seals was a desirable feature for future seal design.

6. The performance of this compressor was significantly poorer than theoretical predictions due to excessive leakage past the thin seal teeth, large mechanical power losses attributed to seal drag and disc friction, and heat transfer from the shaft bearing to the compression process.

The results of this investigation have not produced a suitable seal design or an accurate evaluation of the performance and compression efficiency attainable by a viscous flow compressor with an entirely

circumferential flow path. However, this investigation has isolated several problem areas previously unreported. In order to accurately evaluate the performance of this compressor, the following items are recommended:

1. A new wheel must be accurately manufactured with discs and grooves of uniform thickness, discs perpendicular to the shaft, and negligible axial run-out.

2. A better method of sealing the outside face of the wheel must be developed to reduce the power loss attributed to contact between the wheel and the side casing gasket. A possible solution would be to remove the two outside wheel discs and seal this area with additional stationary seal teeth.

3. The configuration of the experimental apparatus must be modified to thermally isolate the compressor from the shaft bearing and its detrimental heat transfer effects.

4. The surface area of the seal teeth vis-a-vis the wheel should be increased enough to provide an adequate seal and also to provide sufficient rigidity for the teeth to remain fixed under high pressure.

APPENDICES

Table 1. Titanium Wheel Run with Inconel Seals
$T_1 = 69^{\circ}F$ $P_1 = 29.16$ in-Hg = 14.27 psia
Line Pressure = 80 psig

Run	N rpm	P_i psia	P_e in-Hg	T_i $^{\circ}F$	T_e $^{\circ}F$	h_{line} in-H_2O	Q_{line} SCFH
1	10,000	15.37	29.26	73	68	1.6	15,320
2	"	15.37	29.26	73	70	1.6	15,320
3	"	15.37	29.26	73	70	1.6	15,320
4	"	15.37	29.26	73	70	1.6	15,320
5	15,000	16.07	29.46	73	69	2.2	17,960
6	"	16.07	29.46	73	69	2.2	17,960
7	"	16.07	29.46	73	69	2.2	17,960
8	"	16.17	29.46	73	69	2.2	17,960
9	"	16.07	29.46	73	69	2.2	17,960
10	20,000	16.67	29.66	73	65	3.2	21,650
11	"	16.67	29.66	73	65	3.2	21,650
12	"	16.77	29.66	73	65	3.2	21,650
13	"	16.67	29.66	73	65	3.2	21,650
14	"	16.77	29.66	73	65	3.2	21,650
15	24,000	17.57	29.86	73	62	4.4	25,400
16	"	17.57	29.86	73	62	4.5	25,900
17	"	17.57	29.86	73	62	4.4	25,400
18	"	17.57	29.86	73	62	4.5	25,900
19	"	17.77	29.86	73	62	4.5	25,900
20	27,000	18.47	30.06	73	60	5.3	27,900
21	"	18.47	30.06	73	60	5.2	27,350
22	"	18.47	30.06	73	60	5.2	27,350
23	"	18.47	30.06	73	60	5.2	27,350
24	"	18.47	30.06	73	60	5.2	27,350
25	30,000	19.17	30.26	73	58	6.6	31,100
26	"	19.17	30.26	73	58	6.6	31,100
27	"	19.17	30.26	73	58	6.6	31,100
28	"	19.27	30.26	73	58	6.4	30,600
29	"	19.37	30.26	73	58	6.4	30,600
30	35,000	20.77	30.76	73	57	8.2	34,600
31	"	20.57	30.76	73	57	8.4	35,000
32	"	20.77	30.76	73	57	8.3	34,900
33	"	20.77	30.76	73	57	8.5	35,400
34	"	20.77	30.76	73	57	8.3	34,900
35	40,000	22.47	31.36	73	55	11.1	40,300
36	"	22.47	31.36	73	55	11.1	40,300
37	"	22.57	31.36	73	55	11.1	40,300
38	"	22.57	31.36	73	55	11.2	40,400
39	"	22.57	31.36	73	56	11.1	40,300
40	42,000	23.17	31.56	73	55	12.3	42,200
41	"	23.27	31.56	73	55	12.4	42,600
42	"	23.27	31.56	75	55	12.4	42,600
43	"	23.27	31.56	75	56	12.9	43,400
44	"	23.27	31.56	75	55	13.0	43,700

Table 1 Continued

Run	P_a psia	P_b psia	P_3 in-Hg	T_a °F	T_b °F	T_{1fe} °F	h_{1fe} in-H_2O	Q_{1fe} SCFM
1	13.87	13.87	29.41	80	86	82	.8	10.3
2	13.97	14.07	29.47	82	87	82	.7	9.73
3	13.97	14.17	29.54	86	91	83	.5	6.44
4	14.07	14.27	29.66	87	93	83	.3	3.81
5	13.47	13.67	29.41	90	99	94	1.3	15.9
6	13.57	13.87	29.66	92	102	94	1.2	15.23
7	13.57	14.17	29.79	93	104	95	1.0	12.35
8	13.77	14.27	30.04	95	105	95	.8	10.0
9	13.87	14.47	30.28	97	108	95	.4	5.06
10	13.07	13.37	29.54	104	119	113	1.9	21.9
11	13.27	13.97	29.79	107	123	113	1.6	17.4
12	13.37	14.17	30.04	111	127	117	1.4	16.3
13	13.57	14.47	30.41	113	133	119	1.0	11.6
14	13.67	14.52	30.56	117	138	121	0.8	9.41
15	12.67	13.27	29.66	121	146	139	2.3	25.4
16	12.97	13.97	30.16	126	152	142	2.0	21.6
17	13.17	14.27	30.41	128	155	145	1.8	19.3
18	13.27	14.39	30.66	132	159	147	1.4	15.1
19	14.47	14.57	31.54	134	165	150	1.2	13.15
20	12.47	13.17	29.79	138	168	162	2.6	26.3
21	12.77	13.47	30.41	141	173	162	2.2	22.8
22	13.97	14.17	30.54	142	176	165	2.0	20.4
23	13.07	14.37	30.79	143	178	166	1.8	18.3
24	13.17	14.52	31.10	146	182	170	1.6	16.25
25	12.17	13.07	29.79	150	190	182	2.8	25.8
26	12.47	17.77	30.41	153	196	186	2.5	23.5
27	12.67	14.27	30.79	156	202	190	2.2	21.2
28	12.87	14.47	31.16	158	205	193	2.0	18.9
29	13.07	14.67	31.66	161	210	193	1.6	15.4
30	11.87	12.87	29.91	163	216	210	3.3	28.5
31	12.07	13.67	30.66	170	227	215	2.9	24.6
32	12.37	14.27	31.16	172	232	221	2.6	22.2
33	12.57	14.47	31.54	178	240	225	2.2	18.1
34	12.87	14.77	32.16	185	249	227	1.8	15.7
35	11.47	12.57	29.91	188	259	256	3.6	26.6
36	11.67	13.47	30.79	195	270	259	3.2	23.8
37	11.87	13.97	31.16	199	276	265	3.0	22.2
38	12.27	14.52	32.04	206	286	268	2.4	18.8
39	12.47	14.87	32.66	212	298	270	2.0	14.9
40	11.27	12.47	30.04	206	285	281	3.7	25.5
41	11.57	13.27	30.79	210	292	282	3.4	24.2
42	11.77	13.67	31.16	214	300	286	3.2	22.4
43	11.97	14.27	31.66	217	306	289	2.8	19.8
44	12.37	14.97	32.91	227	322	288	2.0	14.75

Table 2. Titanium Wheel Run with Teflon Seals
$T_1 = 69^{\circ}F$ $P_1 = 28.72''$ Hg = 14.1 psia
Line Pressure = 80 psig

Run	N rpm	P_i psia	P_e in-Hg	T_i $^{\circ}F$	T_e $^{\circ}F$	h_{line} in-H_2O	Q_{line} SCFH
1	10,000	-	28.82	73	69	1.5	14,810
2	"	-	28.82	73	69	1.4	14,330
3	"	-	28.82	73	69	1.5	14,810
4	"	-	28.82	73	69	1.5	14,810
5	"	-	28.82	73	69	1.5	14,810
6	15,000	15.9	28.92	73	67	2.0	17,110
7	"	15.8	28.92	73	67	2.0	17,110
8	"	15.9	28.92	73	67	2.0	17,110
9	"	15.9	28.92	73	67	2.0	17,110
10	"	15.7	28.92	73	67	2.0	17,110
11	20,000	16.6	29.12	73	64	3.2	21,650
12	"	16.6	29.12	73	64	3.2	21,650
13	"	16.7	29.22	73	64	3.2	21,650
14	"	16.7	29.22	73	64	3.2	21,650
15	"	16.7	29.22	73	64	3.4	22,300
16	24,000	17.6	29.32	73	64	4.4	25,400
17	"	17.6	29.42	73	64	4.6	26,500
18	"	17.6	29.42	73	64	4.5	25,900
19	"	17.5	29.42	73	64	4.5	25,900
20	"	17.6	29.42	74	64	4.4	25,400
21	"	17.6	29.42	74	64	4.4	25,400
22	"	17.6	29.42	74	64	4.4	25,400
23	"	17.6	29.42	74	64	4.4	25,400
24	27,000	18.3	29.52	74	62	5.2	27,350
25	"	18.3	29.52	74	62	5.2	27,350
26	"	18.3	29.52	74	62	5.2	27,350
27	"	18.3	29.52	74	62	5.2	27,350
28	"	18.3	29.52	74	62	5.2	27,350
29	30,000	19.0	29.72	76	61	6.6	31,100
30	"	19.1	29.72	76	61	6.6	31,100
31	"	19.0	29.72	76	61	6.6	31,100
32	"	19.2	29.82	76	60	7.3	32,650
33	"	19.3	29.82	77	60	7.4	32,900
34	35,000	20.1	30.12	77	60	7.8	33,700
35	"	19.9	30.22	77	61	7.2	32,200
36	"	20.1	30.22	77	61	7.0	31,900
37	"	20.0	30.22	77	61	7.2	32,200

Table 2 Continued

Run	P_a psia	P_b psia	P_3 in-Hg	T_a °F	T_b °F	T_{1fe} °F	h_{1fe} in-H_2O	Q_{1fe} SCFM
1	13.8	13.7	28.97	93	96	88	0.8	9.87
2	13.7	13.8	28.97	93	98	89	0.8	9.85
3	13.8	13.8	28.97	93	99	90	0.8	9.85
4	13.8	13.8	28.97	93	99	90	0.8	9.85
5	13.9	14.3	29.595	95	102	90	0.0	0
6	13.6	13.8	29.22	99	108	99	1.2	14.3
7	13.5	13.8	29.22	100	108	100	1.2	14.2
8	13.5	13.8	29.22	100	109	101	1.2	14.2
9	13.4	13.9	29.22	101	111	102	1.2	14.15
10	13.9	14.47	30.22	108	119	88	0.0	0
11	13.1	14.1	29.72	112	130	121	1.4	15.85
12	13.1	14.1	29.72	114	133	123	1.4	15.80
13	13.1	14.1	29.72	117	135	126	1.4	15.75
14	13.2	14.2	29.85	120	137	129	1.4	15.55
15	13.9	14.9	31.34	131	155	108	0	0
16	13.0	14.23	30.47	132	158	149	1.6	17.0
17	13.0	14.3	30.47	134	159	150	1.6	17.0
18	13.0	14.31	30.47	137	162	151	1.6	16.9
19	13.0	14.35	30.60	138	164	155	1.6	16.7
20	13.2	14.6	30.97	146	173	158	1.2	12.6
21	13.3	14.8	31.34	150	178	156	1.0	10.75
22	13.5	14.9	31.60	152	182	153	0.7	7.65
23	13.9	15.3	32.10	162	196	129	0.0	0
24	12.8	14.35	30.85	150	182	171	1.9	19.5
25	12.8	14.40	30.97	152	183	171	1.8	18.15
26	13.0	14.75	31.47	156	190	174	1.5	15.15
27	13.3	14.95	31.97	159	196	174	1.0	10.3
28	13.8	15.40	32.72	176	221	160	0.0	0
29	12.5	14.4	31.22	164	204	194	2.0	18.9
30	12.5	14.45	31.34	165	207	196	1.9	17.95
31	12.9	14.8	31.85	172	214	194	1.5	14.35
32	13.2	14.9	31.97	190	261	210	1.0	9.25
33	13.5	15.1	32.10	217	296	176	0.0	0
34	12.5	14.3	31.47	200	264	226	1.8	15.4
35	12.7	14.4	31.60	197	260	226	1.4	12.1
36	13.0	14.8	32.34	205	269	222	1.0	9.0
37	13.6	15.3	32.97	230	299	181	0.0	0

Table 3. Titanium Wheel with No Seals
$T_1 = 68^{\circ}F$
$P_1 = 29.31"$ Hg = 14.4 psia
Line Pressure = 80 psig

Run	N rpm	P_i psia	P_e psia	T_i $^{\circ}F$	T_e $^{\circ}F$	h_{line} in-H_2O	Q_{line} SCFH
1	15,000	15.5	14.6	73	67	1.7	15,800
2	20,000	16.5	14.8	73	66	2.2	17.950
3	24,000	17.2	15.0	71	63	3.1	21,320
4	27,000	17.8	15.2	73	63	3.8	23,600
5	30,000	18.5	15.5	73	63	4.4	26,500
6	35,000	19.9	15.9	73	63	6.0	29,650
7	42,000	22.4	16.7	73	61	8.8	35,950

Table 4. Turbine Data with Spacer in Compressor.
$T_1 = 68^oF$ $P_1 = 29.16"$ Hg = 14.32 psia
Line Pressure = 80 psig

Run	N rpm	P_i psia	P_e psia	T_i ^oF	T_e ^oF	h in-H_2O	Q SCFH	T_a ^oF	T_b ^oF	Oil Temp ^oF
1	15,000	15.62	14.57	70	68	1.5	14,810	94	95	-
2	20,000	15.92	14.72	70	68	1.6	15,300	101	102	-
3	24,000	16.62	15.02	70	65	2.2	17,500	111	112	-
4	27,000	17.02	15.12	70	65	2.5	19,150	117	118	130
5	30,000	17.72	15.32	70	65	2.9	20,600	123	126	140
6	35,000	18.42	15.72	68	65	3.3	21,950	134	138	152
7	40,000	19.92	16.22	67	63	4.8	26,500	144	147	160
8	35,000	18.42	15.82	67	63	3.6	22,900	148	151	169
9	30,000	17.52	15.42	67	65	2.6	19,500	149	152	170
10	27,000	17.02	15.12	67	65	2.2	17,500	149	152	170
11	24,000	16.62	15.02	67	65	1.8	16,250	148	151	167
12	20,000	15.92	14.82	68	65	1.4	14,330	146	149	162
13	15,000	15.52	14.62	68	68	1.1	12,700	145	148	159

Table 5. Power Loss vs. RPM for Turbine and Compressor with Titanium Wheel and Inconel Seals

Run	N	*a	*b	*c	*d	*e	*f	*g	*h
	rpm	BLU/hr	BTU/hr	BTU/hr	BTU/hr	BTU/hr	BTU/hr	BTU/hr	BTU/hr
1	15,000	1,482	583	899	1,555	-	121	-	972
2	20,000	3,460	775	2,685	2,450	1,010	277	733	1,675
3	24,000	5,860	1248	4,612	3,380	2,480	405	2,075	2,132
4	27,000	7,140	1382	5,758	4,400	2,740	621	2,119	3,018
5	30,000	9,380	1533	7,847	5,380	4,000	720	3,280	3,847
6	35,000	11,430	1760	9,670	6,320	5,110	1315	3,795	4,560

*a - Power absorbed in Turbine Rotor
*b - Power loss of Turbine Glands and Bearings
*c - Shaft Power to Compressor Rotor
*d - Power loss of Turbine, Windage and Disc Friction
*e - Work of Compression and Seal Drag
*f - Work of Compression Calculated by Friction Factor
*g - Seal Drag Power Loss
*h - Windage and Disc Friction Power Loss

Table 6. Meriam Laminar Flow Element Pressure Correction Factors for Mass Flow Units
Base Pressure = 29.92" Hg, Absolute (see page 12)

Pressure (P_3) Inches Hg. Abs.	28	29	30	31	32
.00	.9358	.9692	1.0027	1.0361	1.0695
.05	.9375	.9709	1.0043	1.0378	1.0712
.10	.9392	.9726	1.0060	1.0394	1.0729
.15	.9408	.9743	1.0077	1.0411	1.0745
.20	.9425	.9759	1.0094	1.0428	1.0762
.25	.9442	.9776	1.0110	1.0445	1.0779
.30	.9459	.9793	1.0127	1.0461	1.0795
.35	.9475	.9809	1.0144	1.0478	1.0812
.40	.9492	.9826	1.0160	1.0495	1.0829
.45	.9509	.9843	1.0177	1.0511	1.0846
.50	.9525	.9860	1.0194	1.0528	1.0862
.55	.9542	.9876	1.0211	1.0545	1.0879
.60	.9559	.9893	1.0227	1.0561	1.0896
.65	.9576	.9910	1.0244	1.0578	1.0912
.70	.9592	.9926	1.0261	1.0595	1.0929
.75	.9609	.9943	1.0277	1.0612	1.0946
.80	.9626	.9960	1.0294	1.0628	1.0963
.85	.9642	.9977	1.0311	1.0645	1.0979
.90	.9659	.9993	1.0328	1.0662	1.0996
.95	.9676	1.0010	1.0344	1.0678	1.1013

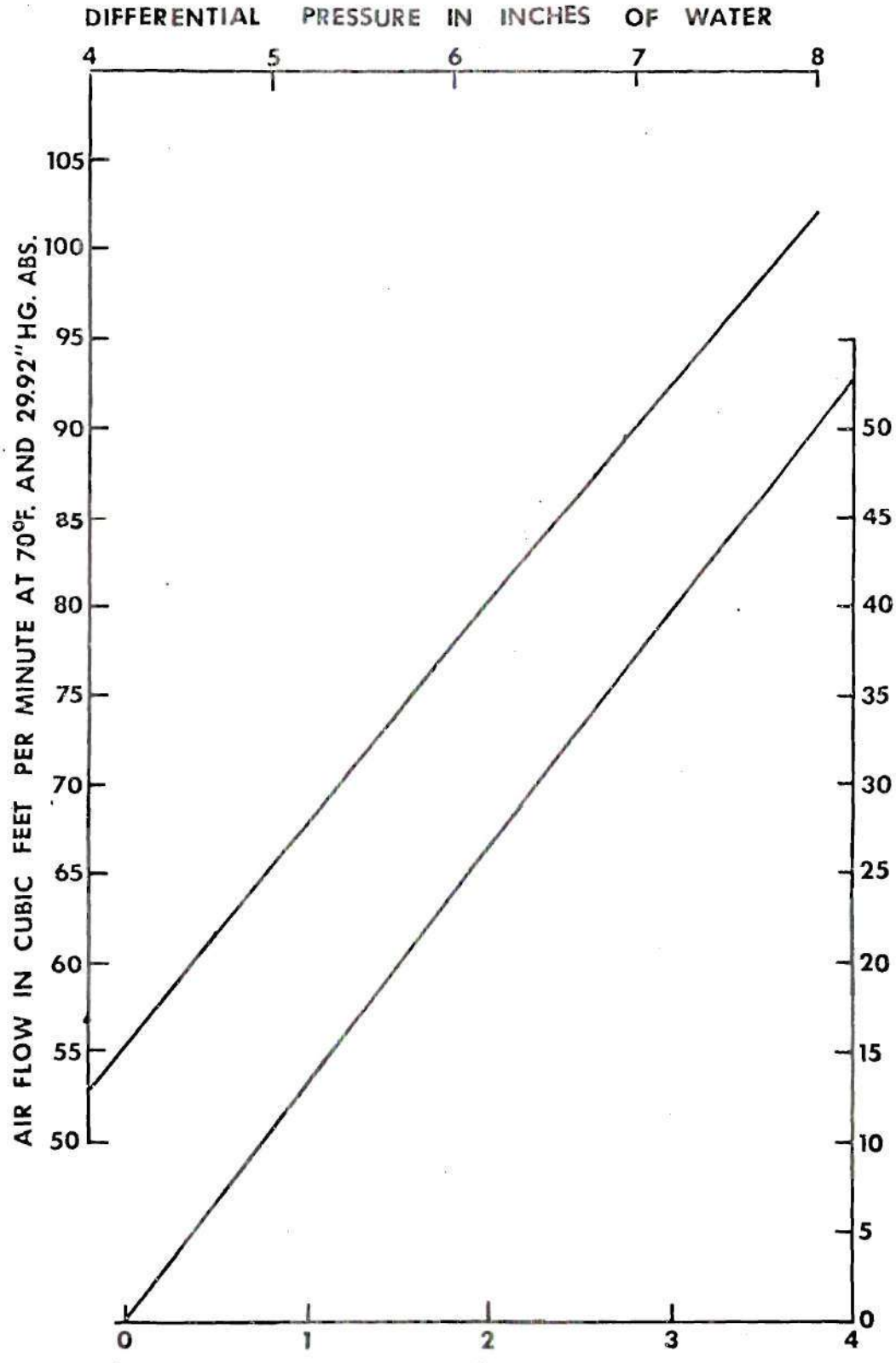

Figure 20. Meriam Temperature Correction Chart.

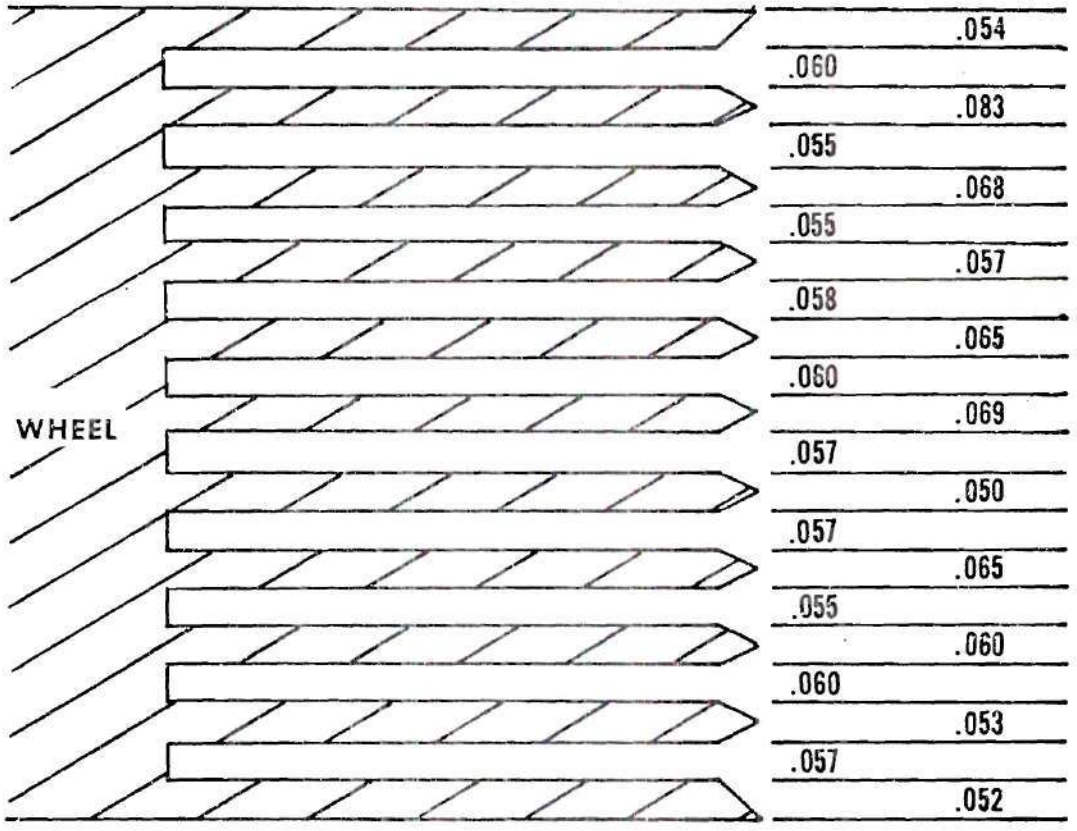

Disc and Groove Dimensions in Inches

Figure 21. Disc and Groove Dimensions.

Appendix C-1. Sample Calculation of the Volume Flow Rate in the Compressed Air Line Feeding the Drive Turbine. (12)

The pipe size of the feed line is 6 40 Standard. Therefore, D = 6.065 inches (Table 5, page 56)

The orifice plate (with flange taps) hole diameter, d, equals 2.426 inches. Therefore,

$$\frac{d}{D} = \frac{2.426}{6.065} = .40$$

The concentric orifice factor, $S_o = 0.099$, for pipe Reynolds numbers in the 8000 to 15000 range (Table 49, p. 150).

$$(A)\ W_h = 45.465\ S_o\ F_a\ D^2 \sqrt{\gamma\ h\ (\gamma_m - \gamma_s)}$$ (Eqn. 11, p. 94)

Where: W_h = mass flow rate (1 bm/hr)

F_a = orifice area correction factor = 1

D = inside diameter of the feed line (inches)

γ = density of the compressed air (1 bm/ft^3)

γ_m = density of the manometer fluid (water @ 70^{o}F)

= 62.27 1bm/ft^3

γ_s = 0

h = differential reading of the manometer (in. - H_2O)

Therefore,

$$W_h = 45.465\ S_o\ F_a\ D^2 \sqrt{\gamma\ h\ (62.27 - 0)}$$

(B) $$W_h = 359.06\ S_o\ F_a\ D^2 \sqrt{\gamma\ h}$$

The compressed air was assumed to be dry. Therefore,

(C) $$\gamma = \frac{2.702\ pG}{TZ} \qquad \text{(Eqn. 16, p. 96)}$$

Where: 2.702 = gas constant = $\frac{0.08073\ (460+32)}{14.7}$ and 0.08073 lbm/ft^3 is the density of pure, dry air at 14.7 psia, and $32^{\circ}F$.

p = absolute gas pressure (psia)

T = absolute gas temperature ($^{\circ}R$)

G = specific gravity of the dry air = 1

Z = super compressibility factor = 1

In order to standardize this development, let

(D) $$Q_h = \frac{W_h}{\gamma_b} = \frac{(W_h)(T_b)}{2.702}$$

Where: γ_b = a base density at T_b and p_b

T_b = a base temperature = $70^{\circ}F = 530^{\circ}R$

p_b = a base pressure 29.92 in.-Hg. 14.696 psia

Q_h = volume flow rate - standard ft^3/hr (SCFH)

Therefore, substituting equations B and C into D

(E) $$Q_h = \frac{(359.06)\ T_b\ S_o\ F_a\ D^2 \sqrt{h}}{2.702\ \ P_b\ G} \sqrt{\frac{2.702\ pG}{TZ}}$$

$$= \frac{(359.06)\ (530)\ (.099)\ (1)\ (36.784)}{(2.702)\ (14.696)\ (1)} \sqrt{\frac{94.7}{(535)\ (1)}} \sqrt{h}$$

and p = 80 psig = 94.7 psia; assume T = $75^{o}F = 535^{o}R$

(F) $Q_h = (12.1 \times 10^3)\sqrt{h}$ SCFH

Appendix C-2. Calculation of Adiabatic Compression Efficiency.

The data used for this calculation were taken from run number 15 with inconel seals installed in the compressor. (See Table 1)

$$\eta_c = \frac{\text{Work required for reversible process}}{\text{Work required for actual process}} \quad \text{(Ref. 9, p. 129)}$$

(A) $$\eta_c = \frac{\Delta h_o}{\Delta h'_o} = \frac{c_p (T_{o3} - T_{o1})}{c_p (T_{o'3} - T_{o1})} = \frac{T_{o3} - T_{o1}}{T_{o'3} - T_{o1}}$$

Since T_{o_3} (the isentropic exit stagnation temperature) and $T_{o'_3}$ (the actual exit stagnation temperature) are in the same range, the specific heats, c_p, are approximately equal.

From the experimental data (Table 1),

$Q_{1fe} = 25.4 \text{ ft}^3/\text{min}$

$T_1 = T_{o_1} = 69^\circ\text{F} = 529^\circ\text{R}$

$P_1 = 29.16 \text{ in.Hg} = 14.27 \text{ psia}$

$P_3 = 29.66 \text{ in. Hg} = 14.58 \text{ psia}$

From air tables (Table 2.4, Ref. 11),

@ $T_1 = 529^\circ\text{R}$, $p_{r_1} = 1.629$

$$\frac{P_3}{P_1} = \frac{P_{r3}}{P_{r1}} \text{ gives} \qquad P_{r_3} = P_{r_1}\left[\frac{P_3}{P_1}\right] = \left[\frac{14.58}{14.27}\right] 1.629 = 1.662$$

@ $P_{r_3} = 1.662$, $T_3 = 532^\circ\text{R}$ (the static isentropic exit temp)

In order to calculate the value of T_{o_3}, one must know the velocity at the exit, V_3. At any point in the flow,

$$T_o = T + \frac{V^2}{2 g_c c_p J}$$ (Ref. 9, p. 104)

and for normal values of temperature, c_p = .24 BTU/1 bm - ^oR, g_c = 64.4 ft - 1 bm/ 1 bf-sec^2, J = 778.2 ft - 1 bf/BTU.

Therefore,

$$\text{(B)} \quad T_o = T + \left[\frac{V}{110}\right]^2 \text{ and } T'_{o_2} = T'_2 + \left[\frac{V_2}{110}\right]^2$$

T'_2 was estimated assuming a linear temperature gradient between points a and b (see Figure 4), which are approximately 5.5 inches apart. Therefore from Table 1,

$$\frac{T_b - T_a}{5.5} = \frac{146-121}{5.5} = 4.55\ ^oF/in.$$

and since point two is one inch from point b,

$$T'_2 \approx T_b + \frac{T_b - T_a}{5.5} = 146 + 4.55 = 150.55^oF = 610.55^oR$$

To calculate V_2, the relation $V_2 = \frac{Q_2}{A_2}$ was used where $Q_2 = Q_{lfe} + .15\ Q_{lfe} = 1.15\ Q_{lfe}$ (assumed 15 percent leakage), and A_2 = (10 grooves)(.06 in.)(.431 in.) = .2586 in.^{2},

$$V_2 = \frac{(1.15)(254)(144)}{(.2586)(60)} = 245 \text{ ft/sec}$$

and substituting this value into equation (B),

$$T'_{o_2} = 610.55 + \left[\frac{245}{110}\right]^2 = 615.5\ ^\circ R$$

The flow in the diffuser between points two and three was assumed isentropic, therefore $T'_{0_2} = T'_{0_3}$.

From one-dimensional compressible flow tables (Ref. 10, Table D-1),

at $\frac{T'_2}{T'_{o2}} = \frac{610.55}{615.5} = .992$, $\frac{A_2}{A^*} = 2.96$.

$$\frac{A_3}{A^*} = A_3\left[\frac{A_2}{A^*}\right]\frac{1}{A_2} = \frac{\pi(.562)(2.96)}{.2586} = 20.2$$ which gives

$\frac{T'_3}{T'_{o3}} = .9998$. Therefore, $T'_3 = (.9998)(615.5) \approx 614^\circ R$

$$T'_{o3} = T'_3 + \left[\frac{V_3}{110}\right]^2 \; ; \left[\frac{V_3}{110}\right]^2 = T'_{o3} - T'_3 = 615.5 - 614 = 1.5^\circ R$$

$$T_{o3} = T_3 + \left[\frac{V_3}{110}\right]^2 = 532 + 1.5 = 533.5^\circ R$$

and substituting into equation (A),

$$\eta_c = \frac{533.5 - 529}{615.5 - 529} = \frac{4.5}{86.5} = .052 = 5.2\ \%$$

Appendix C-3. Turbine and Compressor Power Losses.

1. Power absorbed in the turbine rotor (p_T) with the inconel seals installed in the compressor. The data used for these sample calculations were taken from run 12, Table 1.

From Table 1, $T_i = 73^{\circ}F$; $T_e = 65^{\circ}F$; h = 3.2 in. - H_2O

$$T_{o_i} = T_i + \left[\frac{V_i}{110}\right]^2 \qquad \text{as derived in Appendix C-2.}$$

$$V_i = \frac{Q_h}{A_i} = \frac{121 \times 10^3 \sqrt{h}\ \text{ft}^3/\text{hr}}{(.0533\ \text{ft}^2)(3600\ \text{sec/hr})} = 631\sqrt{h}\ \text{ft/sec}$$

$$V_i = 631\sqrt{3.2} = 113.9\ \text{ft/sec}$$

$$T_{o_i} = 73 + \left[\frac{113.9}{110}\right]^2 = 74.07^{\circ}F = 534.04^{\circ}R$$

$$V_e = \frac{Q_h}{A_e} = \frac{(121 \times 10^3 \sqrt{h}\ \text{ft}^3/\text{hr})(144\ \text{in}^2/\text{ft}^2)}{(5.84\ \pi\ \text{in}^2)(3600\ \text{sec/hr})} = 47.3\ \text{ft/sec}$$

$$T_{o_e} = T_e + \left[\frac{V_e}{110}\right]^2 = 525.18\ ^{\circ}R$$

$$P_T = W_h c_p (T_{o_i} - T_{o_e})$$

$$W_h = Q_h \gamma$$

where γ is the density of air at standard conditions of 70°F, 14.696 psia. Therefore from Appendix C-1,

$$W_h = (12.1 \times 10^3 \sqrt{h}) \left[\frac{2.702 p_b G}{T_b} \right] = (12.1 \times 10^3 \sqrt{h}) \left[\frac{(2.702)(14.696)(1)}{530} \right]$$

$$= 9.06 \times 10^2 \sqrt{h} \text{ lbm/hr}$$

$$P_T = (9.06 \times 10^2) \sqrt{3.2} \ (.24)(534.04 - 525.18) = 3460 \text{ Btu/hr}$$

2. Power loss of the turbine bearings and glands. These data were taken from the runs at 20,000 rpm with a spacer installed in the compressor (Table 4). The average of the inlet and outlet for runs two and twelve were used. From Table 4 , T_i = 69°F; T_e = 66.5°F; h = 1.5 in. - H_2O, and using the same procedure as in part 1,

$$V_i = 63.1 \sqrt{1.5} = 77.3 \text{ ft/sec} \ ; \ V_e = 32.4 \text{ ft/sec}$$

$$T_{o_i} = 529.49°R \ ; \quad T_{o_e} = 526.59°R$$

$$P_T = W_h c_p (T_{o_i} - T_{o_e}) = (9.06 \times 10^2) \sqrt{1.5} \ (.24)(529.49 - 526.59) = 775 \text{ Btu/hr}$$

3. Shaft power delivered to the compressor rotor = (1-2).

   3460 - 775 - 2685 BTU/hr.

4. Power loss of the turbine, windage, and disc friction.

   From run two, Table **3** , with no seals in the compressor,

   $T_i = 73^{\circ}F$; $T_e = 66^{\circ}F$; h = 2.2 in. - H_2O.

   By methods similar to parts one and two,

   $T_{O_i} = 533.72^{\circ}R$; $T_{O_e} = 526.13^{\circ}R$; $P_T = 2450$ BTU/hr.

5. Power loss of the work of compression plus the seal drag = (1-4)

   = 3460 - 2450 = 1010 BTU/hr.

6. Calculation of the power of compression ($\dot{W}$) using the friction factor (f).

(A) $$\dot{W} = \frac{f \rho V_r^2}{8 g_c} u \, (2H + W) \, \Delta z$$ (Ref. 7, p. 10)

Where:

$\dot{W}$ = power to actual compression process (BTU/hr).

f = friction factor.

V_r = (u - V), the velocity of the fluid relative to the rotor (ft/sec).

u = tip speed of the rotor at the mean radius of the grooves.

H = height of the discs above the hub of the wheel.

W = the average width of the grooves.

Δz = 0.708 ft., the distance the fluid travels on the wheel from intake to exhaust.

ρ = the average density (lbm/ft^3)

g_c = 32.174 (ft - lbm/ lbf - sec^2)

Substituting the appropriate values into equation (A),

(B) $$\dot{W} = f \rho V_r^2 \, u \, (9.75 \times 10^{-4}) \quad \text{BTU/hr.}$$

$$\rho = \frac{P_{avg}}{RT_{avg}}$$ where p_{avg} and T_{avg} were taken at the mid-point between points a and b in Table 1 .

$$\rho = \frac{(13.77 \text{ lbf/in}^2)(144 \text{ in}^2/\text{ft}^2)}{(53.34 \text{ ft-lbf/lbm-}^\circ\text{R})(579^\circ\text{R})}$$

The mean radius of the grooves is 3.285 inches.

$$u = \frac{[2\pi(3.285) \text{ in/rev}]\,[N \text{ rev/min}]}{(12 \text{ in/ft})(60 \text{ sec/min})} = 572 \text{ ft/sec}$$

$$V = \frac{1.15\, Q_{lfe}(144)}{(.2586)(60)} = 173.5 \text{ ft/sec}$$

$$V_r = (u - V) = 398.5 \text{ ft/sec}$$

In order to calculate the friction factor (f) one must calculate the relative roughness $\frac{\varepsilon}{D_h}$, where,

ε = the average roughness; assumed to equal .00015 ft., the the roughness for commercial steel.

D_h = hydraulic diameter = $\frac{4 \text{ cross sectional area circumferential flow area}}{\text{section length}}$ (Ref. 10, p. 426)

$D_h = \frac{4HW}{2H+W} = 0.112$ inches. Therefore,

$$\frac{\varepsilon}{D_n} = \frac{(.00015 \text{ ft.})(12 \text{ in/ft})}{0.923 \text{ in.}} = 0.0161$$

To calculate the Reynolds number (R_e),

$$R_e = \frac{\rho(u-V)2HW}{\mu(H+W)} = \frac{\rho(u-V)2HW}{\mu_o\left(\frac{T}{T_o}\right)^{.712}(H+W)} \quad \text{(Ref. 7, p. 11)}$$

$$R_e = \frac{(\rho \text{ lbm/ft}^3)(V_r \text{ ft/sec})(.0517 \text{ in}^2)}{(38\times10^{-8} \text{ lbf-sec/ft}^2)\left(\frac{T}{T_o}\right)^{.712}(.491 \text{ in})(144 \text{ in}^2/\text{ft}^2)(32.2 \text{ ft-lbm/lbf-sec}^2)}$$

$$R_e = 1.805\times10^4$$

From a Moody Chart (Ref. 10, p. 420) @ $\frac{\varepsilon}{D}$ = .0161 and R_e = 1.805 x 10^4,

4f (from this chart) = f (in above formula) = .0485.

Substituting into equation (B),

$$\dot{W} = (.0485)(.0643)(15.9\times10^4)(572)(9.75\times10^{-4}) = 277 \text{ Btu/hr}$$

7. The seal drag power loss = (5-6) = 1010 - 277 = 733 BTU/hr.

8. The combined windage and disc friction power loss = (4-2) = 2450-775 = 1675 BTU/hr.

Appendix C-4. Calculation of Compressor Internal Efficiency (η_{ic}).

$$\eta_{ic} = \frac{\text{Isentropic work}}{\text{Actual work on gas}} \quad \text{(Ref. 11, p. 105)}$$

$$= \frac{c_p(T_{o_3} - T_{o_1})}{\frac{\dot{W}}{\dot{m}_c}} = \frac{\dot{m}_c c_p(T_{o_3} - T_{o_1})}{\dot{W}} \quad \text{where;}$$

$\dot{W}$ is the power input to the gas from the wheel as calculated in Appendix C-3.

$\dot{m}_c$ = mass flow rate through the compressor

= $(1.15)(Q_{lfe})\rho$ and ρ is for standard conditions.

Therefore, using the sample calculations for run 12, Table 1,

$$\eta_{ic} = \frac{5.2\, Q_{lfe}(.24)(32)}{277} = \frac{(5.2)(21.9)(.24)(32)}{277} = 31.5\%$$

Table 7. Properties of Inconel X-750 (13)

a. Composition %:	Ni	C	Mn	Fe	Si	Cu	Cr	Mo	Ti	Cb
	73.0	.04	.70	6.75	.30	.05	15.0	.8	2.5	.85

b. Max. temperature under load: $1500^{\circ}F$

c. Coefficient of Expansion (70 - $1200^{\circ}F$): 8.4×10^{-6} in/in-$^{\circ}F$

d. Stress to Rupture ($1500^{\circ}F$, 100 hours): 30 kpsi
($1500^{\circ}F$, 1000 hours): 17 kpsi

e. Short Time Tensile Strengths ($1500^{\circ}F$): Yield, 0.2% offset 50 kpsi
Ultimate 60 kpsi

f. Melting Range: 2540 - $2600^{\circ}F$

Table 8. Properties of Teflon (14)

a.	Tensile Strength ($77^{o}F$): 2000 - 4500 psi
b.	Flexural Strength ($77^{o}F$): 2000 psi
c.	Coefficient of Expansion ($77 - 140^{o}F$): 5.5×10^{-5} in/in - ^{o}F
d.	Yield Temperature: $< 320^{o}F$
e.	Heat Distortion Temperature, Low Load: $266^{o}F$
f.	Melting Range: Does not melt but starts a gel state at $621^{o}F$

REFERENCES

1. Vojin Popovic, Rodoslav Howat, and Nikola Nikolic, "Nikola Tesla, 1856-1943, Lectures, Patents, Discussions," Nikola Tesla Museum, Boegrad, 1956.

2. J. H. Armstrong. "An Investigation of the Performance of a Modified Tesla Turbine," M. S. thesis, Georgia Institute of Technology, June, 1952.

3. W. Rice, "An Analytical and Experimental Investigation of Multiple Disk Pumps and Compressors," Journal of Engineering for Power, Vol. 85, July 1963, pp. 191-198.

4. W. Rice, "An Analytical and Experimental Investigation of Multiple-Disk Turbines," Journal of Engineering for Power, Vol. 87, January 1965, pp. 29-36.

5. W. M. Gordon, "An Investigation of a Disc-Type Compressor," M. S. thesis, Arizona State University, June, 1965.

6. D. P. Traviss, Georgia Institute of Technology Special Problem (September, 1969) under the supervision of Dr. G. T. Colwell, School of Mechanical Engineering.

7. S. Dusadeenoad. "Characteristics of a Viscous Flow Compressor," M. S. thesis, Georgia Institute of Technology, September 1970.

8. W. D. Clarke, III, Georgia Institute of Technology Special Problem (September 1970) under the supervision of Dr. G. T. Colwell, School of Mechanical Engineering.

9. D. G. Shepherd, Principles of Turbomachinery, (Toronto: The MacMillan Company, 1956) 10th Edition, pp. 125-130.

10. G. Hansen, Fluid Mechanics, (New York: John Wiley and Sons, Inc., 1967) p. 421.

11. Burgess H. Jennings and Willard L. Rogers, Georgia Turbine Analysis and Practice (New York: Dova Publications, 1953) pp. 104-109.

12. C. F. Cusick, Flow Meter Engineering Handbook, (Philadelphia: Minneapolis-Honeywell Regulator Company, 1961).

13. Theodore Baunmeister, Standard Handbook for Mechanical Engineers, Seventh Edition, (New York, McGraw-Hill, 1967) pp. 6-8 and 6-113.

14. Herbert R. Simonds, Archie J. Weith, and M. H. Bigelow, Handbook of Plastics, Second Edition, (New York, D. Van Nostrand Company, Inc., 1949.)